Development of a simulation environment for wireless body area network

JULIEN VIALLE

KTH Signals
Sensors and Systems

Master's Degree Project
Stockholm, Sweden September 2004

IR–SB–EX–0427

Development of a simulation environment for wireless body area network

Julien Vialle

2004-09-03

ROYAL INSTITUTE
OF TECHNOLOGY
Department of
Signals, Sensors & Systems
Signal Processing
S-100 44 STOCKHOLM

KUNGL. TEKNISKA
HÖGSKOLAN
Institutionen för
Signaler, Sensorer & System
Signalbehandling
100 44 STOCKHOLM

Development of a simulation environment for wireless body area network

Julien VIALLE 790130-A270
KTH Advisor: Mats BENGTSSON
IMEC Advisor: Claude DESSET

September 3, 2004

Abstract

Communication systems around the human body offer great perspectives in the future needs of a changing society. They can change the way in which we think about medicine, sports and entertainment and how we experience them. The development of this technology will lead to a Body Area Network, where sensors placed in and around the body can communicate with the outside world using wireless networks and provide medical information. This project includes many research areas: biosensors, nanotechnology, wireless communication, system design technology, …

In this work the simulation of the communication link is treated. With some limitations on the complexity of the system, an end-to-end model was derived, and implemented with Matlab. This model aims at testing different modulation techniques and system architectures, and compares their performances. In the early phase of the development of a Body Area Network, research groups are focusing on the very low power requirement of the sensors. The simulation environment we built in this thesis is a first tool for estimating the power consumption and make comparisons between different systems.

Contents

1 Introduction 4
1.1 Human++ program and Body Area Network 4
1.2 Problem statement 5
1.3 Outline 6
2 Background 7
2.1 Baseband representation 7
2.1.1 Baseband signals 7
2.1.2 Energy and power 8
2.1.3 White noise 8
2.2 Different modulations 9
2.2.1 Linear modulations 9
2.2.2 Non linear modulations 10
2.3 Reception 15
2.3.1 Linear modulations 15
2.3.2 FSK modulation 16
2.3.3 Continuous phase modulation 16
2.4 Performance in AWGN 20
2.4.1 Linear modulations 20
2.4.2 FSK modulation 20
2.4.3 Continuous phase modulation 20
3 System model 22
3.1 VCO phase noise 22
3.1.1 Baseband model 23
3.1.2 Effects of phase noise 24
3.2 Non-linear amplifier 25
3.2.1 Baseband model 25
3.2.2 Effects of the non-linear amplifier 27
3.3 Channel model 29
3.3.1 Measurements 29
3.3.2 Baseband model 30
3.4 Adding noise 30
3.4.1 Power in the simulated system 30
3.4.2 Performance simulation 31
3.4.3 Power simulation 31
3.5 Matlab simulation 32
4 Performance measurements 34
4.1 Minimizing the energy per bit 34
4.1.1 Link budget calculation 34
4.1.2 PA efficiency 35
4.2 Maximizing the burst data rate 36
4.2.1 Regulations and standards 36
4.2.2 Fit to the mask 38
4.3 Tested modulations 39
5 Simulation results 41
5.1 Zigbee 902 band 41
5.2 Zigbee 2400 band 42
5.3 Bluetooth 2400 band 43
5.4 Comparison of the 3 bands 44
6 Conclusions 47
6.1 Summary 47
6.2 Future work 47
7 Abbreviations 49
8 Bibliography 50

1 Introduction

This master thesis project was performed in the Interuniversity MicroElectronics Center (IMEC), located in Leuven (Belgium). The work developed here is in the frame of a more general project led in IMEC, called the Human++ program. A brief presentation of this project is given below, and will help to understand the different problems we tried to answer to in this thesis.

1.1 Human++ program and Body Area Network

A large number of devices for medical, entertainment, comfort and sport applications will make use of sensors and actuator systems in and around the body. Device manufacturers are seeking opportunities to improve the functionality of devices for diagnostics and therapeutics, while at the same time keeping down the cost and improving user convenience.

Ultimately, this technology will lead to the development of a personal body area network (BAN), which provides medical, sports or entertainment functions for the user. The BAN comprises a series of miniature sensor nodes, each of which has its own energy supply, and is also able to communicate with other sensor nodes or with a central node worn on the body. The central node communicates with the outside world by using a standard telecommunication infrastructure such as wireless local area and cellular phone networks. Figure 1.1 shows the structure of a BAN. As a leading Research and Development institute in a broad spectrum of microelectronics and nanotechnology, IMEC has launched a new multidisciplinary program aimed at developing a body area network for health and comfort monitoring. This program is known as the Human++ program.

Figure 1.1: Body Area Network.

In the design of BAN, the power consumption is of major importance. The consumption requirements of the sensor nodes are very severe (<100mW average power consumption). Very long battery lifetimes are the target and the ultimate goal is even to replace the batteries in the sensor nodes by power scavenging techniques,

which use directly the energy of human body to supply the sensors with the required power. All groups working on the Human++ program are at the present time concentrating on the low power consumption issue, and this was also one of the main objectives in this master thesis.

The already considered potential applications of Human++ program are EEG (electroencephalogram), ECG (electrocardiogram), endoscopy, sports monitoring, or medical diagnostics (see Figure 1.2). In collaboration with the University Hospital of Leuven, IMEC has developed a prototype wireless EEG-monitoring system. This is the first step towards a miniature EEG-system that can detect and even suppress an epileptic seizure.

Figure 1.2: Possible applications of Human++ program.

1.2 Problem statement

The aim of this work was to develop a simulation tool for the body area network to get system level comparison of various schemes in terms of power consumption. This objective includes two phases in the development of the simulation. First find an end-to-end model for our communication system, and then get an estimation of the power consumption for different system architectures, using the model previously developed.

Since we are only in the beginning of the Human++ program, we set up some limitations at the start of the work. We restricted the model to a simple communication link from one sensor to one base station. Moreover we were only interested in the power consumed by the transmitter, since, as we mentioned before, the main objective is to get sensors with very low power consumption. The receive base station was supposed to have high power supply.

The solution approach was to implement an end-to-end model of the communication link with Matlab. Even if we have only simple models for some blocks at the present time, we tried to develop a simulation tool as complete as possible. Other groups in IMEC are working on other field of the Human++ program, such as channel modelling or analogue components to use. When they will get new results, the simulation tool will be updated, and we can get more accurate results.

1.3 Outline

Some theoretical background is presented in Chapter 2. The reader could find here a description of different modulation techniques, as well as different receivers used to perform demodulation. Theoretical results on the performance of the different modulations are also listed here. In Chapter 3 we develope the system model describing the communication link. This model includes modulation blocks of the previous chapter and some non-idealities of the real communication system. This chapter ends by an implementation of the end-to-end model in Matlab. Parameters, which influence the power consumption of the transmitter, are identified in Chapter 4. These parameters are combined in order to develop a criterion to measure the performance of a system in terms of power consumption. Chapter 5 gives examples of system comparison we can get with the model we developed. Finally Chapter 6 provides a summary of the thesis and discusses how the work can be extended in the future.

2 Background

The comparison of different systems for the communication link between the sensors and the receive base station is based on the choice of the modulation technique in the system. There exists a large variety of modulation techniques, each one with advantages and drawbacks in terms of performance, bandwidth occupancy or power consumption. In the Human++ program, the choice of technique is still investigated, in order to reach the best trade off between all parameters.

This section will recall some of the most important characteristics of the commonly used modulations techniques. We can find here the basis equations describing each modulation, and used to simulate the different techniques in Matlab. Before presenting the transmission and reception schemes of the modulations, we will shortly review the concept of baseband representation, which will be used in all the simulations later.

2.1 Baseband representation

To transmit digital information through a specific channel, it is necessary to use some type of carrier modulation. The transmitted signal will have its spectrum centred around a carrier frequency f_c, which is chosen depending on the channel. This signal is called a bandpass signal.

However such a signal can always be described by an equivalent lowpass signal, whose spectrum is centred around zero frequency (see [2]). This lowpass signal is called the equivalent baseband signal.

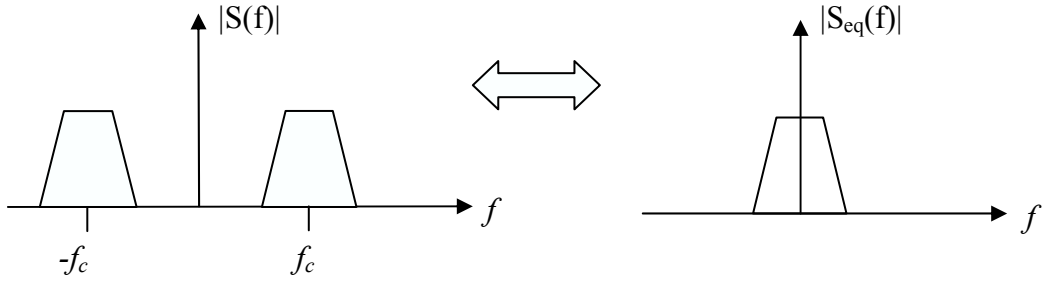

Figure 2.1: Spectrum of bandpass and baseband signals.

While keeping all the information contained in the bandpass signal, the equivalent baseband signal simplifies the communication system simulation and analysis. Therefore in the following all operations will be done on baseband signals.

To make good use of the baseband representation in the following, a brief summary of baseband signals properties is done here. A more detailed presentation of baseband representation can be found in [2].

2.1.1 Baseband signals

The relation between the bandpass signal $s(t)$ and its equivalent baseband signal $s_{bb}(t)$ can be expressed by

$$\begin{aligned} s(t) &= \mathrm{Re}\left[s_{bb}(t) e^{j2\pi f_c t} \right] \\ &= \mathrm{Re}\left\{ \left[s_I(t) + j s_Q(t) \right] e^{j2\pi f_c t} \right\} \end{aligned} \tag{2.1}$$

The signal $s_{bb}(t)$ is in general complex-valued. Its real part $s_I(t)$ is called the in-phase component and its imaginary part $s_Q(t)$ is the quadrature phase component. It can be easier to deal directly with the complex signal or easier to deal with the quadratic components, depending on the situation.

A general modulation scheme can be seen as

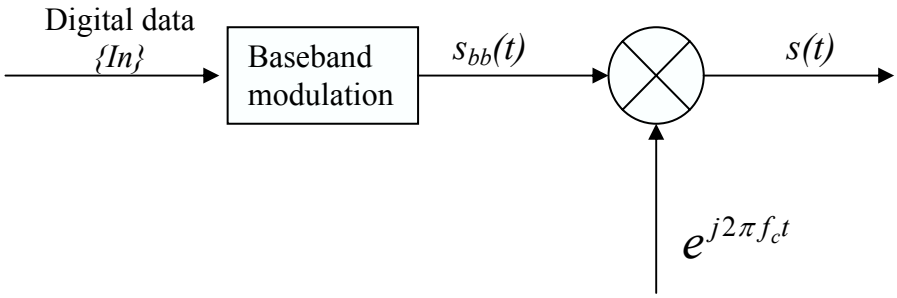

Figure 2.2: General modulation scheme.

Even if the digital modulation can be described by the signal $s_{bb}(t)$, the physical signal which goes through the channel is $s(t)$, and all physical values that are measured are related to $s(t)$. It is therefore important to connect the physical data measured on $s(t)$ to the simulated data, computed with $s_{bb}(t)$.

2.1.2 Energy and power

Due to the baseband representation, all powers and energy are always doubled compared to the physical signals ([2]). The energy of the physical signal is computed from the baseband signal as

$$E_S = \int_{-\infty}^{\infty} |s(t)|^2 = \frac{1}{2} \int_{-\infty}^{\infty} |s_{bb}(t)|^2 \, dt \tag{2.2}$$

For the power, this gives

$$P_S = \frac{1}{2} P_{S_{bb}} = \frac{1}{2} \lim_{T \to \infty} \frac{1}{2T} \int_{-T}^{T} |s_{bb}(t)|^2 \, dt \tag{2.3}$$

2.1.3 White noise

In many communication systems, the signal is polluted by noise. Parameters describing the noise are related to bandpass signal, and need to be transposed to baseband representation. In general, noise added in the communication link is white. It means that noise can be seen as a stochastic process with a constant power spectral density. A complete derivation of how to get the baseband representation of a stochastic process can be found in [2]. The results for white stochastic process are given below.

If $n(t)$ is a white stochastic process with a power spectral density $N_0/2$, the autocorrelation function of $n(t)$ is given by

$$\gamma_{NN}(t) = \frac{N_0}{2}\delta(t) \tag{2.4}$$

The baseband equivalent noise can then be modelled as

$$n_{bb}(t) = n_I(t) + jn_Q(t) \tag{2.5}$$

where $n_I(t)$ and $n_Q(t)$ are two independent white stochastic processes with equal autocorrelation functions

$$\gamma_{N_I N_I}(t) = \gamma_{N_Q N_Q}(t) = N_0\delta(t) \tag{2.6}$$

The complex signal $n_{bb}(t)$ is also white, with an autocorrelation function

$$\gamma_{N_{bb}N_{bb}}(t) = 2N_0\delta(t) \tag{2.7}$$

Taking the Fourier transform of this autocorrelation function shows that the baseband representation of the white noise has a constant power spectral density of $2N_0$.

It was also shown in [2], that if $n(t)$ is gaussian, then $n_I(t)$ and $n_Q(t)$ are two independent gaussian processes. This result will be very useful in Section 3.4, to simulate the noise in the system.

2.2 Different modulations

There are many ways of classifying the modulator, and we chose here to separate the two main categories: linear and non-linear modulations. We will only present here general descriptions of the different modulations. More detailed results can be found in [1] and [2].

The first step of all modulation techniques is to take blocks of $k = log_2 M$ bits and select one of the M symbols I_n. In this work, the assignment between bits and symbols will always use Gray encoding (see [2]). Bits are transmitted at rate R_b bit/s. The time interval between two bits is $T_b = 1/R_b$, and hence the time interval between two symbols is $T = kT_b$. In a second step, a continuous signal, which contains the information symbols, is generated. In general, the continuous signal can be described by a set of coordinates in a signal space defined by basis waveforms (see[2]).

2.2.1 Linear modulations

In linear modulation, the symbol I_n is shaped by a pulse $g(t)$, giving one of the m waveforms

$$s_m(t) = I_n g(t), \quad I_n \in \{A_1, A_2, ..., A_M\} \tag{2.8}$$

In PAM, symbols are real valued, and the signal space is one-dimensional.
In QAM, symbols are complex valued, and the signal space is two-dimensional.

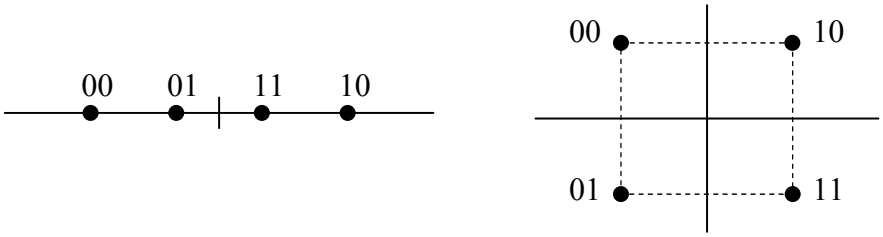

Figure 2.3: Signal space for PAM and QAM.

When a stream of symbols is transmitted, one waveform is emitted every T seconds, and the baseband signal is

$$s(t) = \sum_n s_m(t - nT) = \sum_n I_n g(t - nT) \tag{2.9}$$

The general scheme for linear modulation is represented on Figure 2.4.

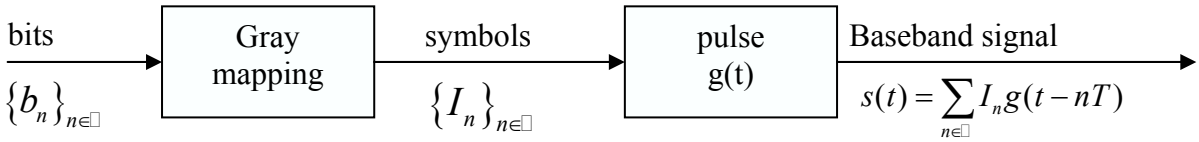

Figure 2.4: Linear modulation scheme.

Many pulses *g(t)* can be used, affecting the spectral characteristics and performance of the modulation. In wireless communications, it is common to use the family of squared root raised cosine pulses. As shown in [1], those pulses avoid Intersymbol Interference (ISI) in the system. Also compared to a simple rectangular pulse of length T (which also avoids ISI), the square root raised cosine keeps the signal power in a narrower band than with a rectangular pulse (see Figure 2.5). So the required bandwidth to transmit the signal will be smaller.

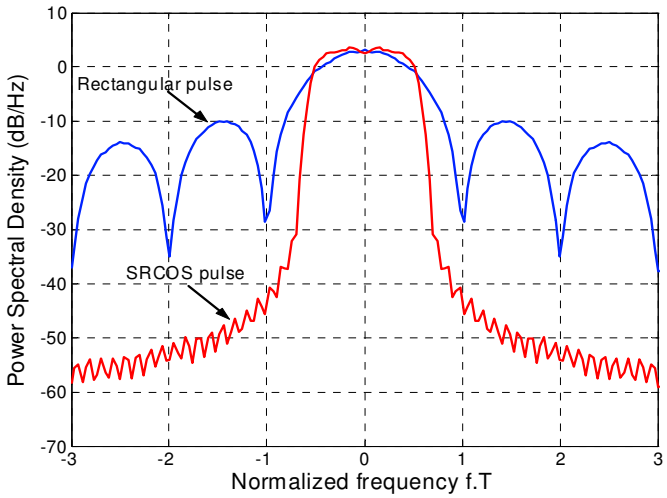

Figure 2.5: Power spectrum for linear modulation

Later on, when using linear modulation, the default pulse will be a square root raised cosine with roll-off $\alpha = 0.3$.

2.2.2 Non linear modulations

The non-linear modulations we will study here are frequency modulations. The digital information is contained in the frequency (or the phase) of the baseband signal. As a consequence, the envelope of the baseband signal is constant. We will first describe frequency shift keying (FSK) modulation, which is a memoryless modulation, and then see a modulation with memory, the continuous phase modulation (CPM).

- FSK modulation

In FSK modulation, the symbol I_n defines the frequency of the baseband waveform. The symbol I_n can take the values

$$I_n \in \{1, 2, ..., M\} \Delta f$$

and the M possible signal waveforms are

$$s_m(t) = \sqrt{\frac{2E}{T}} e^{j 2\pi I_n t}, \quad 0 \le t \le T \tag{2.10}$$

where E is the energy transmitted during one symbol interval.

In the case in which $\Delta f = 1/2T$, the M waveforms are orthogonal ([2]) and the signal space has M dimensions.

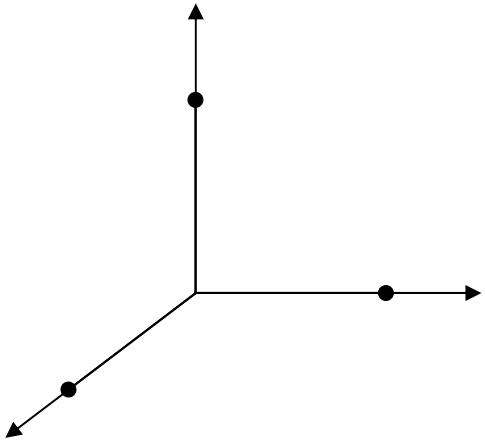

Figure 2.6: FSK signal space for M=3.

When emitting a sequence of digital information $\{I_n\}$, the emitted signal switches from one frequency to another. Such abrupt switching in successive signal intervals results in relatively large spectral side lobes and hence this modulation requires a large frequency band for the transmission. One solution is then to make the frequency change continuously. This kind of modulation is called continuous phase FSK (CPFSK), and is a particular case of the class of continuous phase modulation (CPM).

- Continuous phase modulation

Description of CPM modulation is abundant in the literature ([3]-[6]). For this modulation, the symbol I_n can take the values

$$I_n \in \{-(M-1), ..., -3, -1, 1, 3, ..., (M-1)\}$$

The baseband signal can then be written as

$$s(t) = \sqrt{\frac{2E}{T}} \exp[\phi(t, \underline{I})] \tag{2.11}$$

where the phase $\phi(t, \underline{I})$ is

$$\phi(t, \underline{I}) = 2\pi h \sum_{k=-\infty}^{n} I_k q(t - kT), \quad nT \le t \le (n+1)T \tag{2.12}$$

In this expression, h is called the modulation index, and $q(t)$ is some normalized waveform called the phase pulse. This waveform can in general be represented as the integral of some pulse $g(t)$

$$q(t) = \int_{-\infty}^{t} g(\tau)d\tau \tag{2.13}$$

with the restriction

$$\int_{-\infty}^{\infty} g(\tau)d\tau = \frac{1}{2} \tag{2.14}$$

A conceptual general transmitter structure is shown on Figure 2.7.

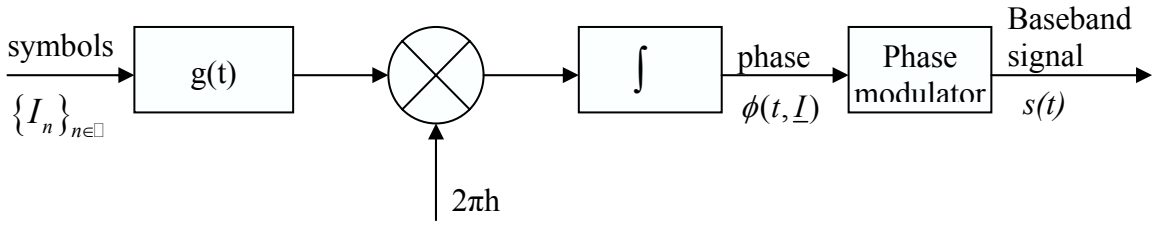

Figure 2.7: Conceptual modulator for CPM signal.

The shape of $g(t)$ determines the smoothness of the transmitted information-carrying phase. Some of the most popular pulse shapes are listed in Table 2-1. In most of the case, the pulse $g(t)$ has a finite length and is zero outside the time interval $0 \le t \le LT$. Then L is the length of the pulse (per unit T).

Name	Phase pulse g(t)	Shape of the pulse with length $L = 2$
LREC	$g(t) = \begin{cases} \frac{1}{2LT} & ,0 \le t \le LT \\ 0 & ,otherwise \end{cases}$ L=1 yields to the special modulation CPFSK.	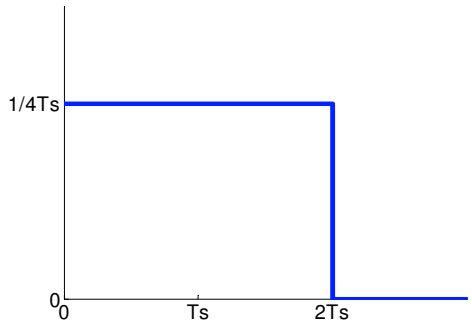
LRC	$g(t) = \begin{cases} \frac{1}{2LT}\left[1-\cos\left(\frac{2\pi t}{LT}\right)\right] & ,0 \le t \le LT \\ 0 & ,otherwise \end{cases}$	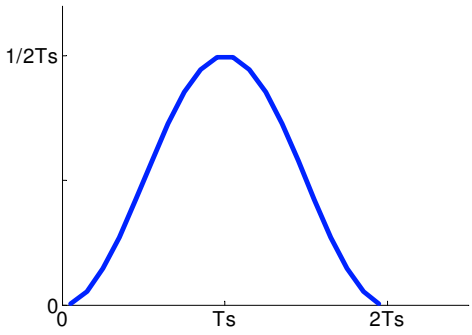

GFSK	$g(t)=\frac{1}{2T}\left[Q\left(\frac{2\pi B}{\sqrt{\ln(2)}}(t-\frac{T}{2})\right)-Q\left(\frac{2\pi B}{\sqrt{\ln(2)}}(t+\frac{T}{2})\right)\right]$ where $Q(t)=\frac{1}{\sqrt{2\pi}}\int_t^{\infty} e^{-\tau^2/2}d\tau$ The parameter *BT* is called the time-bandwidth product and set the shape of the pulse.	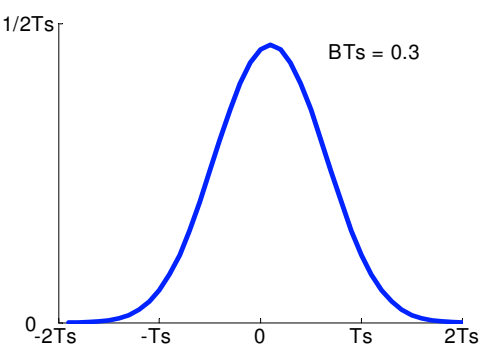

Table 2-1: Pulse used in CPM.

By choosing different pulses *g(t)* and varying the parameters *h* and *M*, a large variety of CPM schemes can be obtained. The widely used modulation Minimum Shift Keying (MSK) can then be seen as a special case of CPM and is obtained by selecting a rectangular pulse of length *L=1*, and using binary data (*M=2*) with *h=1/2*. A detailed description of MSK is given in [17].

The choice of the pulse has important consequences on the spectral characteristics of the signal *s(t)*. Pulses with raised cosine or gaussian shapes give smoother frequency transitions than with rectangular pulse, and result in a more compact power spectrum (see Figure 2.8). Detailed studies on the spectral efficiency of different CPM schemes can be found in [3] or [15].

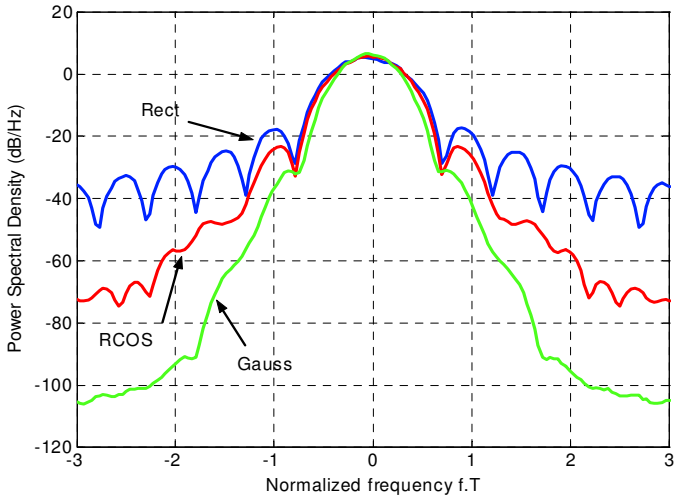

Figure 2.8: Power spectrum for CPM modulation (*h=0.5*).

Memory is introduced into the CPM signal by means of the continuous phase. As it can be seen in Equation (2.12), the phase of the signal *s(t)* between *nT* and *(n+1)T* depends on all the symbols $I_0, I_1, \ldots, I_n$. A finite state trellis structure using this memory can be used to represent CPM signals (see [3]).

For a pulse *g(t)* of length *L* (*g(t)* is zero outside an interval of length *LT*), Equation (2.12) can be written as

$$\begin{aligned}\phi(t,\underline{I}) &= \pi h \sum_{k=-\infty}^{n-L} I_k + 2\pi h \sum_{k=n-L+1}^{n} I_k q(t-kT) \\ &= \theta_n + \theta(t, I_{n-L+1},...,I_n), \quad nT \le t \le (n+1)T\end{aligned} \tag{2.15}$$

Now when h is rational, $h = m/p$, the parameter θ_n can only take certain values (modulo 2π), which are called the phase states

$$\theta_n \in S_\phi = \begin{cases} \{0, \pi h, 2\pi h, ..., (p-1)\pi h\} & ,if\ m\ is\ even \\ \{0, \pi h, ..., (2p-1)\pi h\} & ,if\ m\ is\ odd \end{cases} \tag{2.16}$$

If $L = 1$, Equation (2.15) becomes

$$\phi(t,\underline{I}) = \theta_n + 2\pi h I_n q(t-nT), \quad nT \le t \le (n+1)T \tag{2.17}$$

and we only need to know the phase state θ_n and the symbol I_n to compute the phase of the CPM signal between nT and $(n+1)T$. The states S_n in the trellis are then only defined by θ_n

$$S_n = \left[\theta_n = \pi h \sum_{k=-\infty}^{n-1} I_k \right] \tag{2.18}$$

and the transitions in the trellis are given by

$$S_{n+1} = \left[\theta_{n+1}\right] = \left[\theta_n + \pi h I_n\right] \tag{2.19}$$

An example of such a trellis description of CPM signal is given below, with $h=1/2$.

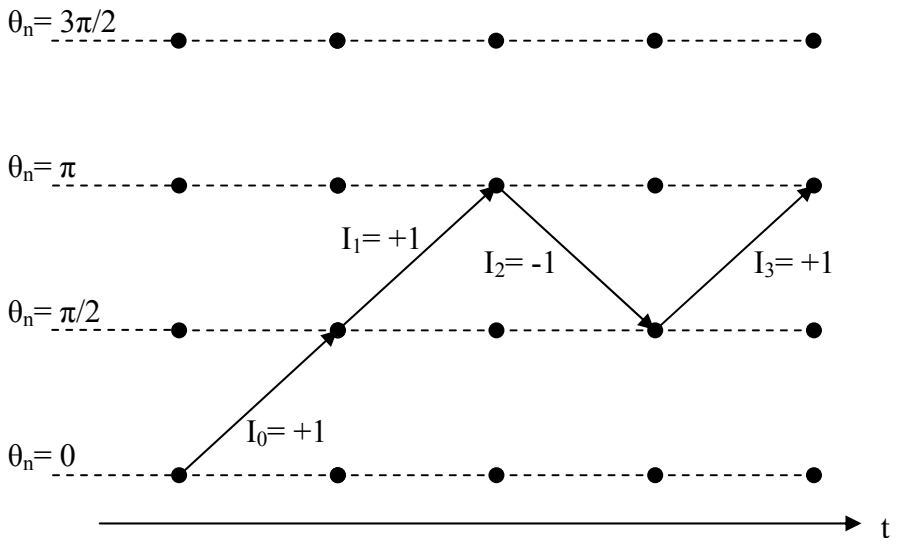

Figure 2.9: Trellis description of CPM signal when $L=1$.

If $L \neq 1$, Equation (2.15) can be written as

$$\phi(t,\underline{I}) = \theta_n + 2\pi h \sum_{k=n-L+1}^{n-1} I_k q(t-kT) + 2\pi h I_n q(t-nT), \quad nT \le t \le (n+1)T \tag{2.20}$$

Knowing the phase state θ_n and the symbols $\{I_{n-L+1}, ..., I_n\}$ the phase of the CPM signal between nT and $(n+1)T$ can be computed from Equation (2.20). A state is then defined as a vector

$$S_n = [\theta_n, I_{n-1}, ..., I_{n-L+2}, I_{n-L+1}] \tag{2.21}$$

and transitions are given by

$$\begin{cases} S_{n+1} = [\theta_{n+1}, I_n, I_{n-1}, ..., I_{n-L+2}] \\ \theta_{n+1} = \theta_n + \pi h I_{n-L+1} \end{cases} \quad (2.22)$$

An example of this trellis structure with *h=1/2* and *L = 2* is given on Figure 2.10. Notice that due to the length of the pulse, the memory is increased and the number of states is doubled.

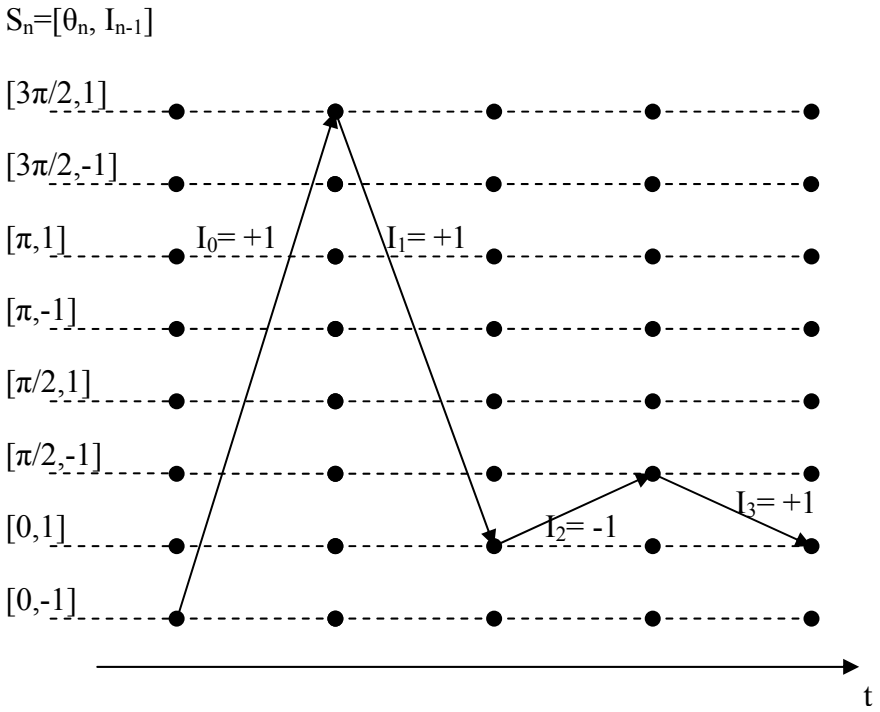

Figure 2.10: Trellis description of CPM with *L=2* and *h=1/2*.

In both cases, the number of states describing a CPM signal is

$$Ns = \begin{cases} pM^{L-1} & if\ m\ is\ even \\ 2pM^{L-1} & if\ m\ is\ odd \end{cases} \quad (2.23)$$

The trellis description of CPM signal implies that a maximum likelihood detector using Viterbi algorithm can be used at the reception, as we will see in the following.

2.3 Reception

Above we described some of the most common modulation techniques, to map digital information into a continuous signal. At the receiver end, we want to get the digital information back from a polluted version of the modulated signal. The derivation of optimum receivers for signals corrupted by the addition of gaussian noise can be found in [2]. Here is a summary of the different receivers that can be used for the different modulations.

2.3.1 Linear modulations

For PAM as for QAM, the optimum receiver can be implemented with a matched-filter, follow by a detector.

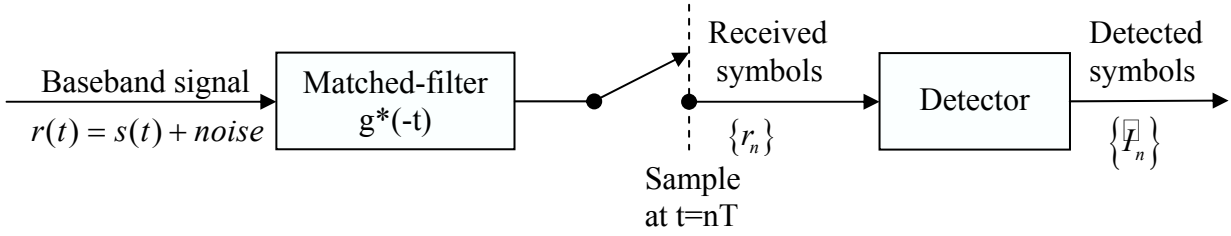

Figure 2.11: Reception scheme for linear modulation.

The output of the matched filter is sampled at $t = nT$, to get the decision variable r_n. The detector compares the decision variable to all possible emitted symbols, and chooses the one, which is the closest (in Euclidean distance).

2.3.2 FSK modulation

We consider the case of M-ary orthogonal FSK signals. The M possible waveforms $s_m(t)$ (see Equation (2.10)) are used in M matched filters to produce the decision variables.

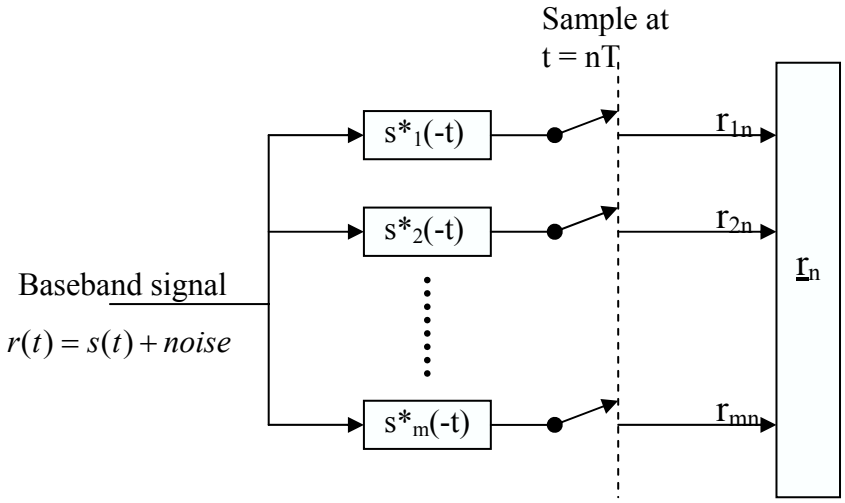

Figure 2.12: Matched filter for FSK.

The vector $\underline{r}_n$ is then used to decide which was the emitted symbol.

If we use coherent detection (the phase of $r(t)$ is known), the vector $\underline{r}_n$ is used for ML detection and the detector selects the symbol corresponding to the closest signal to $\underline{r}_n$ (in the M dimensional signal space). In that case, we need to keep Δf larger than $1/2T$ to ensure orthogonality.

If we use non-coherent detection (unknown phase in $r(t)$), the vector $\underline{r}_n$ is used for envelope detection and the detector selects the symbol corresponding to the maximum $|r_{mn}|$. In that case, the condition to maintain orthogonality is $\Delta f \geq 1/T$.

2.3.3 Continuous phase modulation

CPM is a modulation with memory, since the continuous phase at a time nT depends on all the previous emitted symbols (see Section 2.2.2). Taking this memory into account leads to an optimum receiver based on a maximum-likelihood sequence detector (see [2]).

The complexity of this receiver has lead to the development of sub-optimum receivers, which don't take advantage of the memory of CPM signal, but which are easier and less expensive to realize ([19]-[21], [23]).

- Optimum receiver and Viterbi detector

The maximum likelihood sequence detector uses the trellis structure of the CPM signal and searches the paths through the trellis for the minimum Euclidean distance. This search is efficiently performed with the Viterbi algorithm ([7], [22]).

Observing the received signal $r(t)$ on an interval $0 \le t \le (N+L-1)T$, the Viterbi algorithm will find the most likely emitted symbols sequence $\{I_0, I_1, \ldots, I_N\}$. The algorithm searches in the trellis the most likely states sequence and use the following metrics to measure the likelihood of a transition from state $S_n = i$ to state $S_{n+1} = j$

$$v_n(i,j) = \mathrm{Re}\left[\int_{nT}^{(n+1)T} r(t)\exp\left[-j\phi_{ij}(t,\underline{I})\right]dt\right] \tag{2.24}$$

with

$$\phi_{ij}(t,\underline{I}) = \theta_n^i + \sum_{k=n-L+1}^{n-1} I_k^i q(t-kT) + I_n^j q(t-nT) \tag{2.25}$$

At the end the algorithm selects the states sequence corresponding to the maximum cumulated metrics and deduces the symbols sequence from it.

The drawback with this algorithm is the complexity of the optimum detector. We recall from Section 2.2.2 that the number of states describing the CPM signal is $N_s = pM^{L-1}$ (or $Ns = 2pM^{L-1}$). At each time nT, MN_s metrics are computed (corresponding to all possible transitions) and N_s surviving states sequences are stored. Thus the amount of storage is proportional to the number of states and the amount of computation to the number of transitions.

The number of states can rapidly become important. For instance, a quaternary 5RC system with $h=3/4$ will use 2048 states at the receiver. With such a system, the complexity of the receiver makes it very difficult to implement in practice.

Several simplified Viterbi detectors are proposed in the literature ([8]-[11]). They can significantly reduce the complexity of the receiver at a small penalty on the performance. In this work, we used a simple reduced states Viterbi decoder. When the number of states was too high, the algorithm only stores, at each time interval, the N states sequences corresponding to the N highest cumulative metrics ($N \le N_s$). Thus only MN metrics computations are required at each step.

The reduction of states saves time in the computation while keeping good performances at the reception. An example is given below, for a quaternary 3RC system with $h = 3/4$ (128 states). Table 2-2 summarizes the computation time used by the Viterbi algorithm in Matlab, while Figure 2.13 shows the performance curves obtained with the different states reductions. Of course reducing the number of states leads to a greater amount of detection errors, but we can see that, with at least 20 surviving states, the detector keeps good performances, while the computation time is reduced by 40%.

Number of surviving states	Matlab simulation time for the Viterbi algorithm (in sec)
$N = N_s = 128$	705
$N = 40$	542
$N = 20$	418
$N = 10$	248

Table 2-2: Computation time for the reduced states Viterbi algorithm.

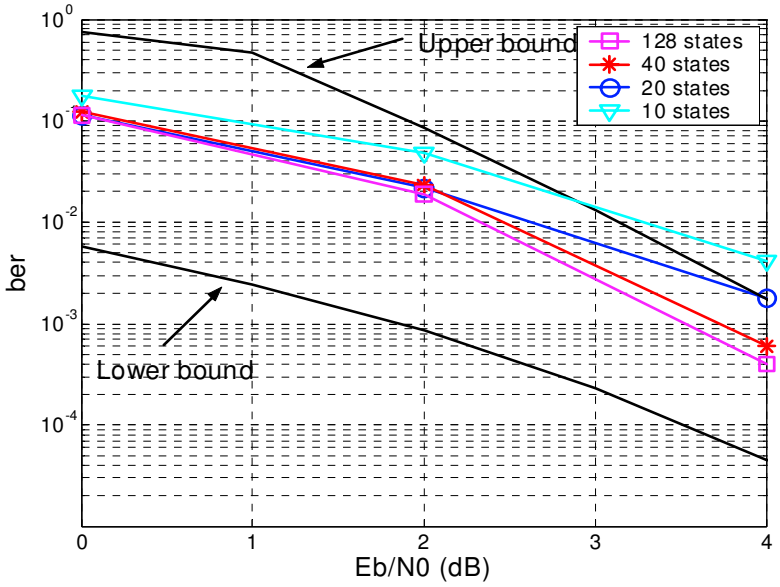

Figure 2.13: BER degradation for reduced states Viterbi algorithm.

- Limiter Discriminator

Due to the complexity of the Viterbi detector, other receiving systems have been developed. Those systems using uncoherent detection are easier to implement and require less computation. Analysis of their performances can be found in [19] and [21].

We only present here an ideal Limiter-Discriminator (LD) receiver. This receiver doesn't take into account the memory of CPM, and only performs frequency demodulation on the signal. Description of different FM demodulators can be found in [1] and [20].

The Limiter aims at removing any amplitude perturbations, which the signal might have undergone in the channel. It produces a constant envelope signal at the input of the Discriminator. This one can be seen, in the ideal case, as a differentiator followed by an envelope detector. The output of the discriminator will be proportional to the instantaneous frequency, (i.e.) the derivative of the phase, of the received signal.

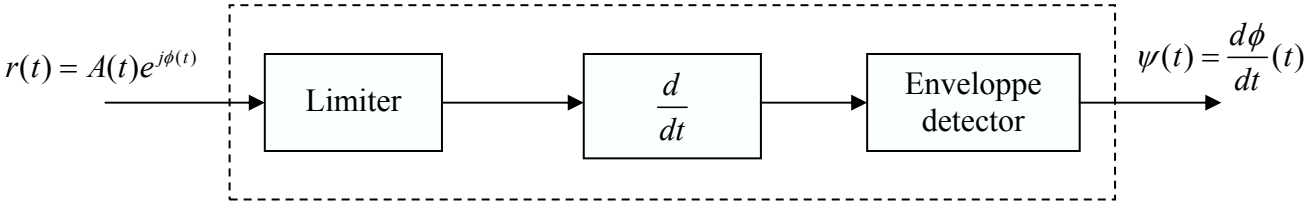

Figure 2.14: Ideal limiter-discriminator receiver.

The phase of the CPM signal is given by Equation (2.12). With this signal, and in the absence of noise, the output of LD receiver will be

$$\psi(t,\underline{I}) = \frac{\partial\phi}{\partial t}(t,\underline{I}) = 2\pi h \sum_{k=-\infty}^{n} I_k g(t-kT), \quad nT \le t \le (n+1)T \qquad (2.26)$$

The ISI introduced by the transmitter shaping filter *g(t)* can be corrected by the same processing methods used for linear modulation in AWGN channel, although these methods are no longer optimum. A detailed description of Limiter Discriminator receiver for CPM signal, including the post detection filtering can be found in [23].

Figure 2.15: Limiter-discriminator receiver for CPM.

Such a detector doesn't offer as good performances as coherent Viterbi detector. An example for MSK modulation is given on Figure 2.16. However it avoids the use of a phase synchronization process, and requires less computation than the Viterbi detector. Its simplicity to implement makes it a very low power-consuming receiver, and is the reason why it is still used in practice.

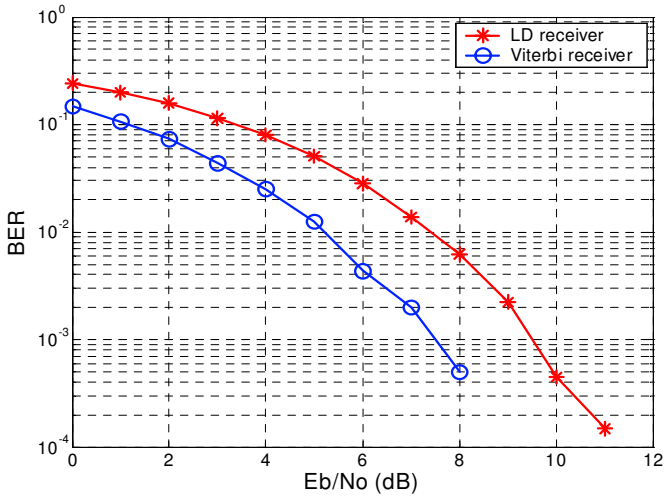

Figure 2.16: BER for MSK with different detectors.

The transmitters and receivers we presented above will be used later in simulations to get a comparison of the system performance for different modulations. All the

described modulations have been extensively studied and theoretical results of their performance have been found. These results were very useful to validate our simulation and to get an ideal case as reference.

2.4 Performance in AWGN

One common performance measure of a communication link is the bit error rate (BER), probability of making an error on one bit. In the case where the only distortion due to the channel is the add of gaussian noise, the BER can be found theoretically as a function of the ratio E_b/N_0, where E_b is the energy received during the transmission of one bit and $N_0/2$ is the spectral density of the added white noise. The derivations can be found in [2], and we only recall the results here.

Notice here that, since we always used Gray mapping, the bit error rate P_b was approximated from the symbol error rate P_m by

$$P_b = \frac{1}{M} P_m \tag{2.27}$$

where M is the number of symbols.

2.4.1 Linear modulations

For M-PAM modulation, the symbol error probability is given by

$$P_m = \frac{2(M-1)}{M} Q\left(\sqrt{\frac{6\log_2 M}{M^2-1}}\sqrt{\frac{E_b}{N_0}}\right) \tag{2.28}$$

where $Q(t) = \frac{1}{\sqrt{2\pi}} \int_t^\infty e^{-\tau^2/2} d\tau$

M-QAM can be seen as two independent PAM modulations, with M_I and M_Q symbols on the two orthogonal dimensions. The symbol error probability is then calculated with the formula for PAM modulation

$$P_m = 1 - (1 - P_m^{M_I - PAM})(1 - P_m^{M_Q - PAM}) \tag{2.29}$$

2.4.2 FSK modulation

For coherent detection and orthogonal signals we have

$$P_m = \frac{1}{\sqrt{2\pi}} \int_{-\infty}^{\infty} \left[1 - \left(1 - Q(y)\right)^{M-1}\right] \exp\left[\frac{1}{2}\left(y - \sqrt{\frac{2\log_2 ME_b}{N_0}}\right)^2\right] dy \tag{2.30}$$

For uncoherent detection the symbol error rate becomes

$$P_m = \sum_{n=1}^{M-1} (-1)^{n+1} \binom{M-1}{n} \frac{1}{n+1} \exp\left[-\frac{n\log_2 M}{n+1}\frac{E_b}{N_0}\right] \tag{2.31}$$

2.4.3 Continuous phase modulation

The computation of CPM performance signal using coherent Viterbi detector is based on the trellis structure of the signal. An error path in the trellis $\underline{\gamma_N}$ is defined as a vector with the difference between the two symbols sequences corresponding to the two paths of length N

$$\underline{\gamma_N} = \{\gamma_1, \gamma_2, ..., \gamma_N\}, \quad with\ \gamma_i \in \{0, \pm 2, \pm 4, ..., \pm 2(M-1)\} \tag{2.32}$$

As shown in [24], the upper bound on symbol error rate is given by

$$P_m < \sum_{\underline{\gamma_N}} w_d Q\left(\sqrt{d^2(\underline{\gamma_N})\frac{E_b}{N_0}}\right) \tag{2.33}$$

where $d(\underline{\gamma_N})$ is the normalized Euclidean distance corresponding to an error $\underline{\gamma_N}$

$$d^2(\underline{\gamma_N}) = \frac{\log_2 M}{T_s}\int_0^{NT}[1-\cos\phi(t,\underline{\gamma_N})]dt \tag{2.34}$$

and w_d is the symbols weight distribution corresponding to error event $\underline{\gamma_N}$ (see [24]). For large value of E_b/N_0, the asymptotic symbol error rate is controlled by d_{min}

$$P_m \approx w_{d\,\min} Q\left(\sqrt{d^2_{\min}\frac{E_b}{N_0}}\right) \tag{2.35}$$

with

$$d^2_{\min} = \lim_{N\to\infty}\left[\min_{\underline{\gamma_N}} d^2(\underline{\gamma_N})\right] \tag{2.36}$$

An algorithm to compute the value of d_{min} is given in [5]. The value of d_{min} is an indicator of the performance of CPM systems and can be used to compare different CPM schemes. It is also a good way to find the best parameters (modulation index and pulse shape) for a given system. This question of optimizing CPM signals is more detailed in [14], [16], [18]. Here we give as an example the d_{min} value for CPFSK modulation was computed as a function of the modulation index h (see Figure 2.17). Maximum value for minimum distance, and thus good performance in BER, are obtained for $h \approx 0.7$. On the contrary, modulation index $h = 1$ gives really bad results, and should be avoided.

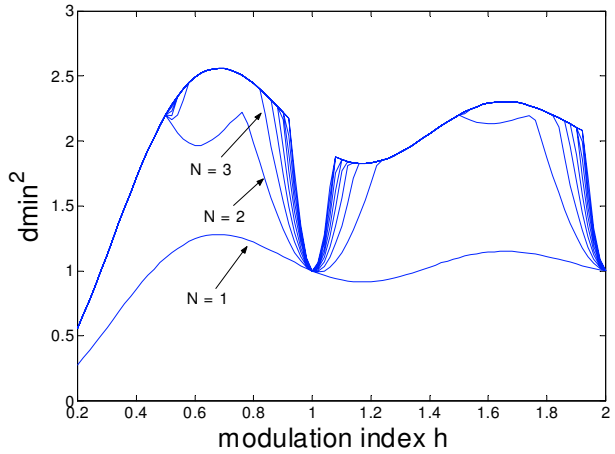

Figure 2.17: Minimum distance in the trellis for CPFSK modulation.

Other bounds for CPM systems can be investigated and founded in [12] and [13].

Transmitters and receivers we described previously have now to be integrated in a more realistic model of our communication system. Non-idealities introduced by the system will degrade the performances of the different modulations. The ideal performances given above will let us quantify this degradation.

3 System model

In a communication system, the baseband-modulated signal transports the information from the transmitter to the receiver. This transmission is done through a specific channel, which set boundary conditions in terms of radiated power and use of the spectrum. The original signal is thus transformed in order to fit to the channel. This transformation is performed by the analog front-end. A general model of the system is depicted on Figure 3.1, and is the same as in [29].

The modulated signal generated by the baseband modulator will undergo many distortions. Distortion will occur during the transmission of course, when passing through the channel. But the analog front ends, used in the transmitter and the receiver, present some non-idealities, which will also distort the signal. This section will present the models we used in this work for the different imperfections of the system and their effects on the modulated signal.

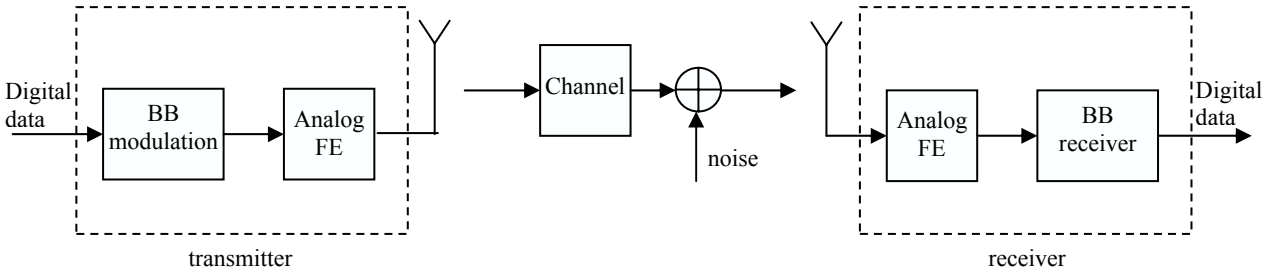

Figure 3.1: System overview.

Most system studies investigate the performance of communication systems without taking into account the impact of the analog front-end. This is equivalent to assuming that the analog front-end is almost perfect and introduces negligible distortion. However, systems operating at low distortion usually require high power consumption, and it can be more efficient to have some distortion, to keep a low power level.

In our model we simulated two types of front-end imperfection: a non-ideal oscillator used to generate the carrier signal and a non-ideal amplifier used at the transmitter to reach a certain power. We still used here a baseband model for the signal and all the distortions will thus be defined on the baseband representation, and the carrier frequency f_c will not appear in the modelling.

3.1 VCO phase noise

A Voltage Controlled Oscillator (VCO) is used in the front-end to generate the carrier waveform. For an ideal oscillator, the output can be expressed as

$$V_{out}(t) = A\cos(2\pi f_c t + \phi) \tag{3.1}$$

with A and Φ constant.

In practical oscillator however, the output takes the form

$$V_{out}(t) = A\cos(2\pi f_c t + \phi(t)) \tag{3.2}$$

where *Φ(t)* is now a function of time, called the phase noise. The output of the VCO presents small variations around the oscillation frequency due to this phase noise. They are several ways of modelling the phase noise process ([30]-[31]). We used here a model based on the Power Spectral Density (PSD) of the phase noise.

Recall from Section 2.1.1, the carrier waveform is used to generate the bandpass signal *s(t)* as follow

$$s(t) = \mathrm{Re}\left[s_{bb}(t) e^{2\pi j f_c t} \right] \tag{3.3}$$

However, due to phase noise, the phase of the carrier is not fixed and the bandpass signal becomes

$$s(t) = \mathrm{Re}\left[s_{bb}(t) e^{2\pi j f_c t + j\phi(t)} \right] \tag{3.4}$$

So the equivalent complex baseband signal affected by phase noise is

$$x_{bb}(t) = s_{bb}(t) e^{j\phi(t)} \tag{3.5}$$

With a model for *Φ(t)*, the baseband distortion causes by the phase noise is thus simply simulated by multiplying the modulated signal by *exp[jΦ(t)]*.

3.1.1 Baseband model

The model for phase noise is taken as a random gaussian process with a piece-wise linear PSD, as shown on Figure 3.2. It comes from the analysis of Phase Locked Loop (PLL) systems, used in the oscillators ([32]). The model includes a flat level close to the carrier frequency, representing the PLL floor, a flat low level representing the system noise floor, and a transition in between with a slope of –20dB/decade. This model is widely used in the literature ([25]-[29]), and corresponds quite well with measurements ([28]).

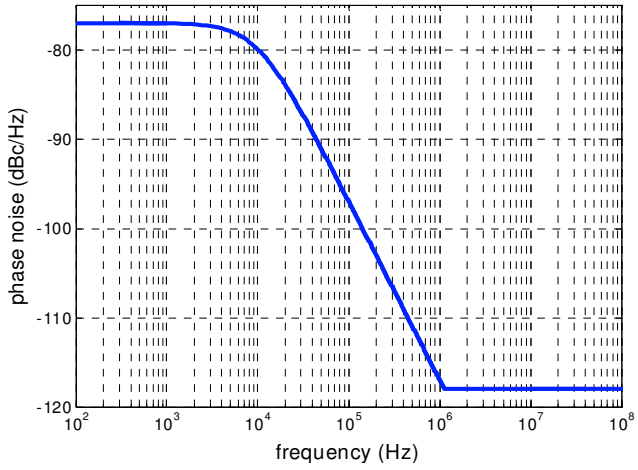

Figure 3.2: Phase noise spectrum.

The values used to define the phase noise spectrum are the one from [29], and are the one we used for all the simulations

PLL noise floor	*-78.2 dBc/Hz*
PLL bandwidth	*10kHz*
System noise floor	*-118 dBc/Hz*
Total integrated phase noise	*-32 dBc*

Table 3-1: Phase noise PSD parameters.

The phase noise generated with these values is then a random gaussian variable with a probability density function shown in Figure 3.3.

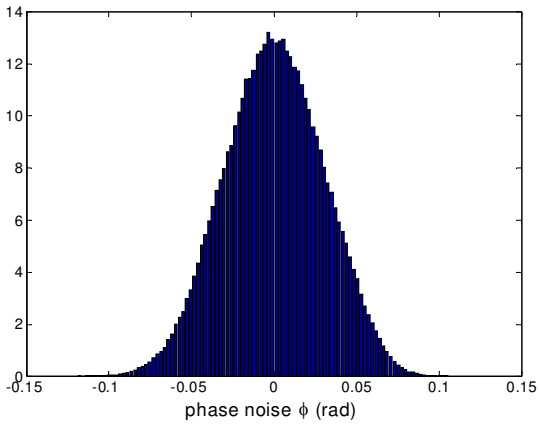

Figure 3.3: PDF of the phase noise.

Even if the random phase keeps relatively small values (between –0.1 and 0.1 radian), it can affect and deteriorate the performance of different modulations schemes.

3.1.2 Effects of phase noise

The random phase introduced by the VCO will affect both linear and non-linear modulated signal. In the case of linear modulation, the effect can be seen on the signal constellation. The unknown phase doesn't change the amplitude of the modulated signal and results in a rotation of the constellation. An example for 64-QAM modulation is shown on Figure 3.4.

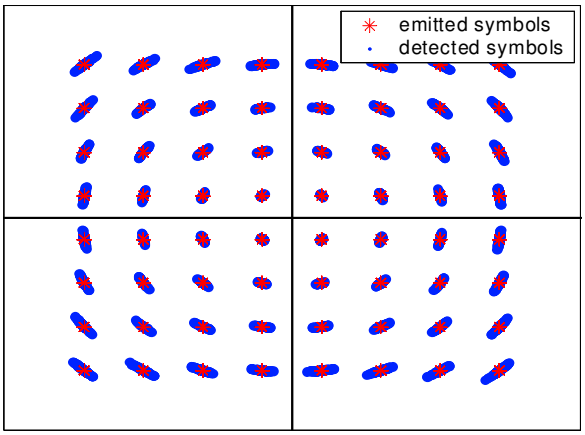

Figure 3.4: 64QAM constellation with phase noise.

This distortion of the signal constellation will then degrade the BER performance of the system. The rotation of the symbols in the constellation decreases the distance from one symbol to the closest decision region border. Thus for a same amount of added white noise, there will be more errors when VCO introduces phase noise than in the ideal case (see Figure 3.5).

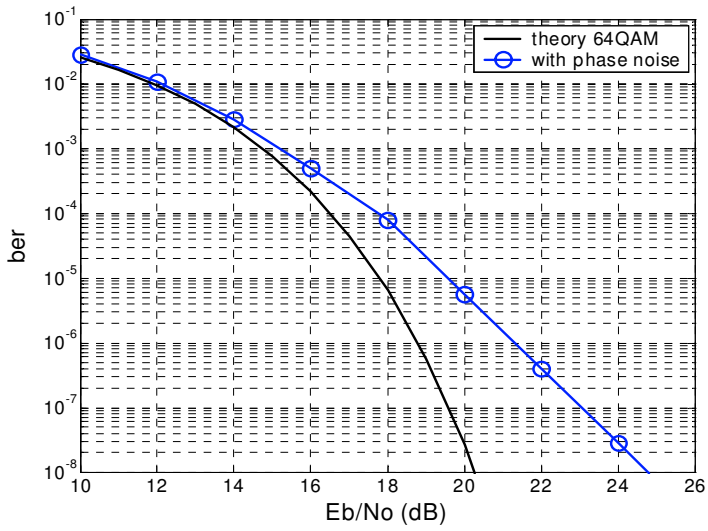

Figure 3.5: BER degradation due to phase noise.

For non-linear modulation, phase noise will also results in a degradation of the BER performances, since it disturbs the phase of the modulated signal, which carries the information. There is not an easy representation of this disturbance as in the case of linear modulation with signal space.

3.2 Non-linear amplifier

In order to reach a desired power level, the modulated signal is amplified. The power amplifier used for this operation can introduce non-linear effects, which will, as phase noise, distort the modulated signal and result in a degradation of the BER. We will present here the model we used to simulate the power amplifier distortion and some examples showing the effects of this distortion on the modulated signal.

3.2.1 Baseband model

Many power amplifier models have been developed ([34], [36]). A general amplitude-phase model of the amplifier gives the following relations between the input signal *x(t)* and the output signal *y(t)*

$$\begin{cases} x(t) = A(t)\exp\left[j\varphi(t)\right] \\ y(t) = G\left(A(t)\right)\exp\left[j\varphi(t) + j\Phi\left(A(t)\right)\right] \end{cases} \tag{3.6}$$

where *G(x)* is the AM-to-AM conversion and *Φ(x)* is the AM-to-PM conversion. Those two functions define the model for the power amplifier and are used to make the simulations ([31]).

Studies about the influence of AM-PM conversion can be found in [35], [37]. But it can be shown by computer that the effect of AM-AM conversion is usually much more significant than the one of AM-PM conversion ([38]). Thus in this paper we always used $\Phi(x) = 0$.

A common model for the AM-AM conversion is to use a cubic non linearity ([29]), with a function *G(x)* defined by

$$G(x) = \begin{cases} G(x - \frac{3}{4}\alpha x^3) & , for\ 0 < x < x_{sat} \\ y_{sat} & , x \geq x_{sat} \end{cases} \quad (3.7)$$

where G is the linear gain and α is the non linearity coefficient, which can be expressed as

$$\alpha = \frac{1}{3x_{sat}^2} \quad (3.8)$$

The curve representing the amplitude transfer function of the PA is then given on Figure 3.6. The reference power P_{ref} is defined as the intersection point between the ideal curve of linear power amplifier and the saturation power $P_{sat} = |y_{sat}|^2$

$$P_{ref} = \frac{|y_{sat}|^2}{G} \quad (3.9)$$

We can set the linear gain to one latter on, since we are only looking at the distortion in the power amplifier.

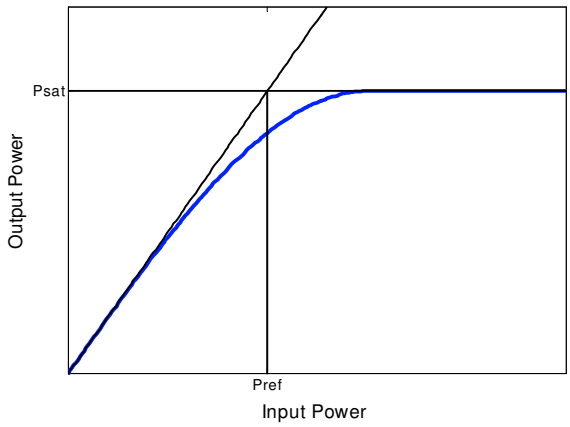

Figure 3.6: AM-AM conversion.

The transfer function above features three regions: a linear region when the input power is somewhat below P_{ref}, a saturation region when the input power is somewhat beyond P_{ref}, and a transition region between. The linearity of the power amplifier operation will thus depends on the input backoff *b*, defined as

$$b = \frac{P_{ref}}{P_{in}} \quad (3.10)$$

Large input backoff results in a good linearity of the power amplifier, whereas small input backoff results in high non-linearity. The input backoff is also an interesting parameter since it has a direct impact on the power consumption of the amplifier, as we will see in Section 4.1.2.

The PA model for baseband simulation can then be defined with this only parameter. From Equation (3.9), and assuming $G = 1$, we have

$$y_{sat} = \sqrt{bP_{in}} \quad (3.11)$$

Combining this result with Equation (3.6) and Equation (3.7) the output of the PA can be expressed as

$$y(t) = \begin{cases} x(t)\left[1 - \frac{9}{64}|x(t)|^2\right] & , for\ |x(t)| \le \frac{4}{3}\sqrt{bP_{in}} \\ \mathrm{sgn}\left(x(t)\right)\sqrt{bP_{in}} & , otherwise \end{cases} \quad (3.12)$$

where P_{in} is the average power of the input signal $x(t)$.

This model was used to simulate the distortion experienced by the baseband signal for different input backoff. Performances of systems using non-linear amplifier can be found in [35]. We present here some examples to illustrate the effects of these non-linearities.

3.2.2 Effects of the non-linear amplifier

We should first notice that in our model, the power amplifier only distorts the amplitude of the baseband signal. Since non-linear modulations have a constant envelope, they will not be affected by the PA.

We chose as an example a 16-QAM modulation, and used an input backoff of 0dB for the amplifier. Because of the saturation of the PA, the signal amplitude is clipped. On the signal constellation, this means that the symbols with the highest energy have their modulus decreased (see Figure 3.7). The global result is a compression of signal constellation.

Figure 3.7: 16QAM constellation with non-linear PA.

This compression decreases the distance between the symbols and the decision region borders, especially for the high-energy symbols. This results in an important degradation of the BER performance of the system (see Figure 3.8).

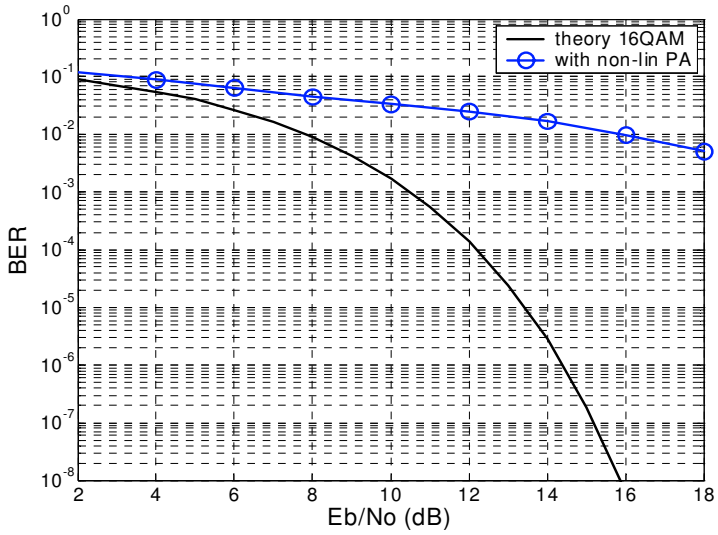

Figure 3.8: BER degradation due to non-linear PA.

Another effect of the non-linear amplifier, which will be important for our system, is the widening of the signal spectrum occupancy. The saturation of the amplifier will create side lobes in the power spectral density of the modulated signal, which consequently uses more bandwidth than in the ideal case (see Figure 3.9).

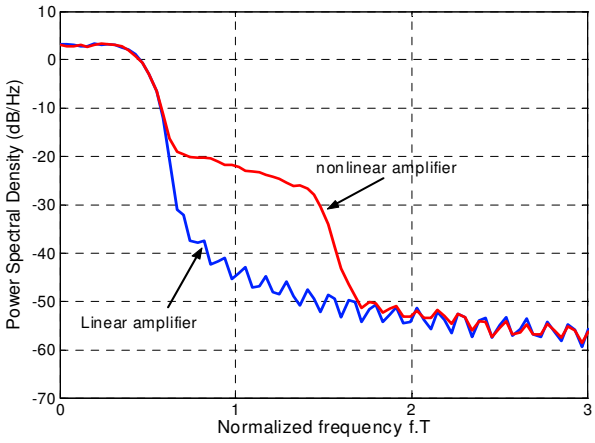

Figure 3.9: 16QAM spectrum with non-linear PA.

The effects described on this example will be as much important as the power amplifier operates in a non-linear region, that is to say as the input backoff is small. The influence of the input backoff on linear modulations can be remembered as:

> The more backoff you have, the less errors you have (for a given E_b/N_0 at the receiver).
>
> The more backoff you have, the less bandwidth you use.

Contrary to phase noise, which we modelled as a given distortion of the system, the distortion introduced by the power amplifier can be modified with the input backoff parameter. The impact of the non-linear power amplifier will be discuss in Section 4 and we will see how we can choose the input backoff in order to get optimal performances for linear modulations.

The phase noise and the non-linear amplifier were the two non-idealities we considered in the analog front end on Figure 3.1. As we can see on this figure, we still have to get models for two system blocks: the channel and the noise addition.

3.3 Channel model

The understanding of propagation around the human body is necessary to develop a specific channel model for our system. Some studies about the influence of human body on signal propagation have already been published ([39]-[41]), and IMEC is currently working on developing its own channel model as a part of the Human ++ project. For that, channel measurements are made: both transmit and receive antennas are placed directly on the body and channel parameters are extracted. The position of the antennas, on the front side of the body or around the upper torso (see Figure 3.10), will give a large amount of data to find a suitable propagation model.

Figure 3.10: Antenna position for channel measurements.

For now, only measurements of loss of power experienced by the transmitted signal are available, and we had to use a relatively simple model for the channel.

3.3.1 Measurements

The antennas were placed around the waist, the transmit antenna in the front of the body, and the receive antenna shifted from a certain angle. The measurements were made for different angle and different carrier frequency. The path loss of the channel is extracted from measurements

$$L = \frac{transmitted\ \ power}{received\ \ power} \tag{3.13}$$

The results can be seen on Figure 3.11.

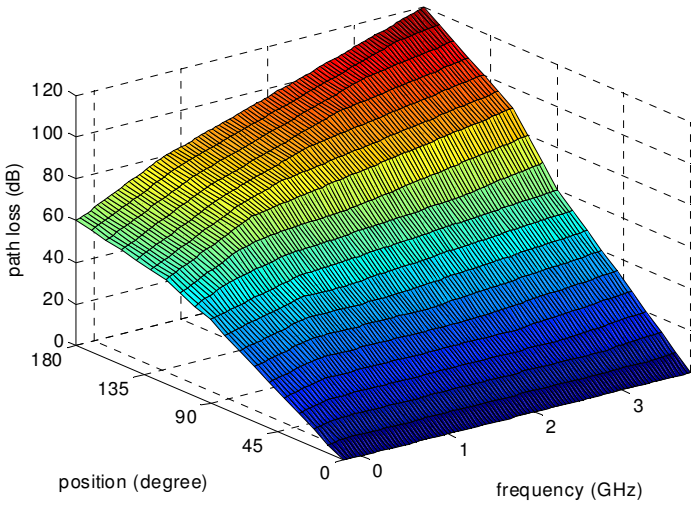

Figure 3.11: Path loss measurements.

The loss of power due to the propagation is of course increasing with the angle between the two antennas. But we also notice that this loss increases with the frequency of the carrier. As we will see in Section 4.2, the choice of the carrier frequency, which determines the choice of the frequency band used by the system, can only be made among a limited set of frequencies. Thus the path loss for a given system will depend on this frequency band selection, and we can get comparisons between systems working at different frequencies.

3.3.2 Baseband model

Since the path loss is a ratio between two powers, there is no difference when dealing with baseband signals or bandpass signals. We use directly the measurements presented above, and the effect of the channel on the emitted signal can be written as

$$\tilde{e}(t) = \frac{e(t)}{\sqrt{L}} \tag{3.14}$$

The last step of the model is now to add noise to this attenuated signal.

3.4 Adding noise

The noise model is a classical additive white gaussian noise, with a power spectral density $N_0/2$. This model is simulated in baseband representation by a complex white gaussian noise with a power spectral density $2N_0$ (see Section 2.1.3). The received signal is

$$r(t) = \tilde{e}(t) + n(t) \tag{3.15}$$

The value of the constant N_0 was computed with two different methods, depending on the type of simulation. To understand how the calculation was done in the simulation, we should first make some remarks about energy and power computations of sampled signals.

3.4.1 Power in the simulated system

When working with digitally sampled signals, as in Matlab, the signal powers are directly computed from the signal samples. Assume a signal *s(t)* of duration T seconds

is sampled at a frequency $f_s = 1/T_s$. The number of samples is then $N=T/T_s$. The power of the signal is given by

$$P_s = \frac{1}{T}\int_0^T |s(t)|^2 \, dt \approx \frac{1}{T} T_s \sum_{n=1}^{N} |s(nT_s)|^2 = \frac{1}{N}\sum_{n=1}^{N} |s(nT_s)|^2 \tag{3.16}$$

The last term is simply the mean of the squared amplitude of the samples, noted σ_s^2. Assuming that the sampling rate is high enough, so that the integral can be approximated by the summation without too much error, the power of the continuous signal can be computed from the sampled signal.

3.4.2 Performance simulation

For this simulation, we want to reach a given E_b/N_0 at the receiver, where E_b is the amount of signal energy received during the transmission of one bit. The value E_b/N_0 is a known parameter, noted as

$$\rho = \frac{E_b}{N_0} \tag{3.17}$$

The power of the received signal in the absence of noise is calculated from the signal *e(t)* as follow

$$P_{Rx} = \frac{\sigma_{\tilde{e}}^2}{2} \tag{3.18}$$

The factor *2* comes from the baseband representation (see Section 2.1.2). The energy per bits is then given by

$$E_b = P_{Rx} T_b = \frac{\sigma_{\tilde{e}}^2}{2} \frac{T}{\log_2(M)} \tag{3.19}$$

where T is the symbol interval and M the number of symbols.

The value of N_0 is computed as

$$N_0 = \left(\frac{1}{\rho}\right) \frac{\sigma_{\tilde{e}}^2}{2\log_2(M)} T \tag{3.20}$$

This way of computed N_0 is used when we want to study the performance of a modulation scheme, and get the bit error rate at the receiver for a given E_B/N_0. But when simulating real systems, we have to deal with real given values of transmitted power and noise power.

3.4.3 Power simulation

We assume for this simulation that the power of the transmitted signal P_{Tx} is known and the baseband-simulated signal is normalized such as

$$\sigma_e^2 = 2P_{Tx} \tag{3.21}$$

Then the energy per bit at the receiver is

$$E_b = \frac{P_{Tx}}{L} \frac{T}{\log_2(M)} \tag{3.22}$$

The value of N_0 is computed by considering all noise sources in the system and by finding the total noise power at the receiver. In our model, we add two gaussian noise sources in the channel:

The thermal noise, whose power is

$$N = kTB \tag{3.23}$$

where k is the Boltzman's constant, T is the temperature, and B is the channel bandwidth. This represents the lowest noise floor for an ideal receiver.

The interference noise, whose power is

$$P_I = IN \tag{3.24}$$

The constant I is a parameter of the system, which is defined as the ratio between the power of the interferences and the power of the thermal noise. Interferences can be seen as all the signals emitted in the same frequency band as our signal. Measurements can be done to estimate the I parameter, and the interferences' level. Typical value for I would be about 12 dB.

Those two noise sources are added, and the total gaussian noise has a power

$$P_{total} = N + P_I = kTB(1+I) \tag{3.25}$$

To finish, the losses and the noise in the receiver itself will increase the noise floor. The noise figurer N_f is a measurement of the power of the noise added by the receiver. It is defined as the ratio between the noise power at the output of the receiver and the noise power at the input of the receiver. A typical value for a low cost receiver will be about 10 dB. Then the noise power at the receiver is

$$P_{noise} = N_f kTB(1+I) \tag{3.26}$$

The value of the power spectral density of the white noise is therefore

$$N_0 = \frac{P_{noise}}{B} = kT(1+I)N_f \tag{3.27}$$

With this value for N_0, and the value of E_b given by Equation (3.22), we can simulate a real system and get the actual E_b/N_0 ratio at the receiver. This kind of simulation requires knowledge about the system, in terms of transmitted power and noise power and is used when we need to know what are the real signals passing trough the channel or what are the signals in the receiver.

3.5 Matlab simulation

The system model presented on Figure 3.1 was simulated with Matlab. The equations described in Section 2.2 were used to get the baseband modulated signals. Then the non-idealities were added using the results of Sections 3.1 and 3.2. The noise was added as a white gaussian noise with variance $2N_0$, and N_0 was computed with one of the two methods presented above. A global scheme for the link model used in this study is shown on Figure 3.12.

Notice that the emitted signal was normalized such as its power was equal to a known transmitted power. So at the transmitter we can use symbols and filters of unit energy to perform the modulation, and only consider the distortion effects in the power amplifier, disregarding the amplification itself. At the receiver, the inverse operation is done to get back the original modulated signal, and same filters of unit energy can be used.

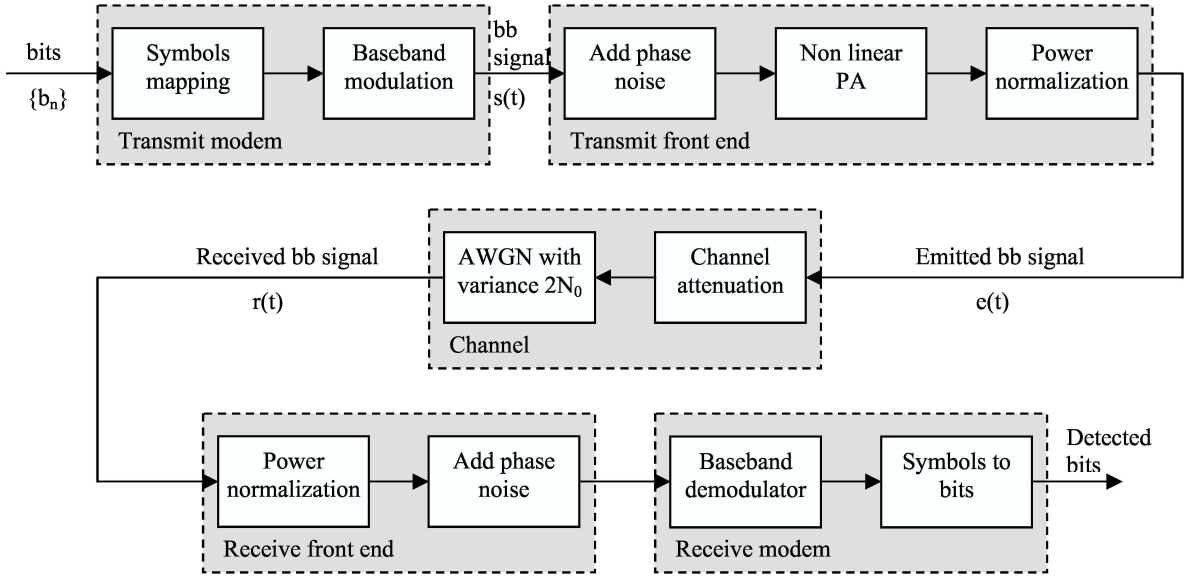

Figure 3.12: Schematic of the system model used in Matlab.

A Matlab function was written to simulate each block of Figure 3.12, and a script links all the blocks together. The simulator can then easily be adapted, by writing new functions simulating new blocks and insert them in the global script.

With this simulation model we can now make a complete analysis of the communication link we are studying. The models for phase noise and channel attenuation are fixed and taken from measurements described in Sections 3.1.1 and 3.3.1. They are considered as characteristics of our system. We can modify the modulation parameters and the non-linearity in the power amplifier to find optimal performances and make comparison between different systems. Results are given in Section 5. In the following section we will see how we estimate the performances of the system.

4 Performance measurements

In the Human ++ program, the key parameter of the system is the power consumption. The sensors placed around the body must have very low power consumption, while they are emitting signals with enough power to reach a required signal to noise ratio at the receiver. To make good comparison of systems, we assume that the average bit rate of the transmitter is always the same, and minimizing power consumption is equivalent to minimizing required energy.

One way to reduce the power consumption is to study the performances of different systems. To reach a fixed BER at the receiver, some system configurations need less energy per bits at the transmitter. The calculation of the energy per bits at the transmitter is explained in Section 4.1.

Another crucial technique to reduce the power consumption is to operate the radio in burst mode: the sensor is not emitting continuously, but only during a time T_{burst}. Therefore analog components of the front end, such as oscillators or mixers, only consume power during that time, and the average power consumption is decreased. On the other hand the effective bit rate is increased, in order to keep the same average bit rate. Limitation on maximum bit rates will be presented in Section 4.2.

4.1 Minimizing the energy per bit

The computation of the required energy per bit at the transmitter will take two parameters into account: the minimum BER we want to reach to get acceptable performance and the efficiency of the power amplifier. The derivation of the total energy per bit is explained below.

4.1.1 Link budget calculation

We assume here that we know the required ratio E_b/N_0 at the receiver to reach a fixed BER. This can be done with the Matlab model we presented in Section 3.5, and by adding the noise as in Section 3.4.2. A simple link budget calculation can be expressed as

$$E_{b-Tx} = \frac{E_b}{N_0} + N_0 + L + L_a \tag{4.1}$$

where L is the channel attenuation, N_0 is the noise power spectral density at the receiver, and L_a is the antenna loss. All values are expressed in dB.

The antenna loss is a measure of the power loss in the antenna due to ohmic dissipation (see [47]). The value of L_a takes into account both losses at the transmit and receive antenna. A typical value is about 3dB.

With the same notation as in Section 3.4.3, the noise power spectral density is given by

$$N_{0|dB} = 10\log_{10}(kT(1+I)N_f) = 10\log_{10}(kT) + 10\log_{10}(1+I) + N_{f|dB} \tag{4.2}$$

In our case, we chose constant values for T, I, N_f and L_a (Table 4-1). The energy per bit will depend on the system performance E_b/N_0 and the path loss of the channel, described in Section 3.3.

Temperature	$T = 290K$
Interference factor	$I = 12\ dB$
Noise figure	$N_f = 10\ dB$
Total noise power spectral density	$N_0 = -211.7\ dBm$
Antenna Loss	$L_a = 3\ dB$

Table 4-1: Link budget parameters.

This calculation provides the required energy per bit at the input of the transmit antenna, to reach a desired BER at the reception side. But the required energy at the transmitter is higher, due to the power consumed by the amplifier to transmit one bit.

4.1.2 PA efficiency

All the power consumed by the amplifier is not converted to the RF signal power. The waste of power is related to the efficiency of the amplifier, defined as

$$\eta = \frac{P_{out}}{P_{dc}} \tag{4.3}$$

where P_{out} is the power of the output signal and P_{dc} is the power supplied to the amplifier. For an ideal amplifier, the efficiency is one. Thus, the power of the output signal is equal to the power taken from the DC supply. In this case, no power would be consumed in the amplifier. In reality, this is not possible, and there will always be some wasted power. This waste of power implies that we need higher energy per bit at the transmitter than the energy required at the output of the transmit antenna.

Taking into account the PA efficiency, the total energy per bit is given by

$$E_{b-tot} = \frac{E_{b-Tx}}{\eta} = E_{b-Tx|dB} - 10\log_{10}(\eta) \tag{4.4}$$

The PA efficiency depends on the linearity of the amplifier. Achieving high linearity requires high DC power and results in low efficiency. So the efficiency is directly related to the input backoff of the amplifier. In a simple class A model ([33]), the efficiency is limited to 50%, and can be expressed as

$$\eta = 0.5P_{norm} \tag{4.5}$$

where P_{norm} is the output signal power, normalized to a saturation power of one. Figure 4.1 shows the efficiency of the power amplifier as a function of the input backoff. The efficiency rapidly decreases as the input backoff increases.

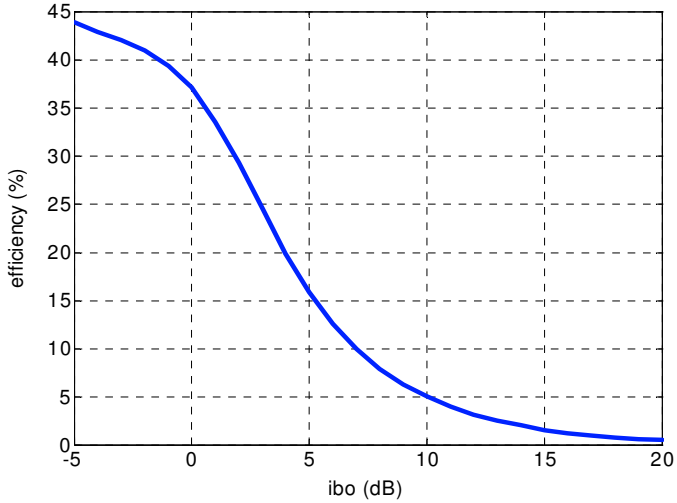

Figure 4.1: Typical class A power efficiency.

The input backoff of the amplifier is therefore an important parameter. Recall from Section 3.2.2 that the BER performance of linear modulations is improved with high input backoff. But this leads to high power consumption in the power amplifier. This trade-off between performances and power consumption for linear modulations will be discuss in Section 5.

For non-linear modulation, we showed that the non-linearities of the amplifier didn't influence the performances. Thus we can work with other classes of amplifiers, which introduce more amplitude distortion but offer higher efficiency. In our simulations we will use a power efficiency of 80% when working with non-linear modulations.

Taking back the values of Table 4-1, and using them in equation (4.1), the power consumption of our system will be minimized by minimizing the energy

$$E_{b-tot} = \frac{E_b}{N_0} - 179 + L - 10\log_{10}(\eta) \tag{4.6}$$

4.2 Maximizing the burst data rate

To reduce the use of front end at the transmitter, the system only transmits information during a time T_{burst}. The burst data rate, which is the effective rate of the transmitted bits, is thus higher than the average bit rate. The shorter T_{burst} is, the higher the rate is, and the lower power consumption is. Therefore a criterion to decrease the power consumption is to maximize the bit rate during transmission.

For a given E_b/N_0 at the receiver, increasing the bit rate will result in an increase of the required bandwidth and of the transmitted power. There exist some limitations in terms of available bandwidth, spectrum pollution, or transmitted power, set by local authorities in each country. We will present here the limitations we chose in the simulations, and how we can find maximum bit rates under those limits.

4.2.1 Regulations and standards

Regulations exist and limit the use of the bandwidth. In the advancement of the Human ++ program, some specific authorized frequency bands are envisaged. They correspond to spectrum bandwidth allowed for short range devices transmission, and are defined by regulatory organisations such as the Federal Communication

Commission (FCC) for the United States, or Electronic Communications Committee (ECC) for Europe. FCC documents ([43]) and ECC documents ([42], [44]) define the rules to follow in terms of maximum transmitted power and spurious emissions.

In addition to those regulations, there already exist standards for Wireless Local Area Networks. The two we studied here are the Zigbee ([45]) and Bluetooth ([46]) standards. The interesting part of those standards for the Body Area Networks is that they define different channel spacing in each frequency band and a spectral mask for each channel. Actually the frequency bands allowed by regulatory organisations can be rather wide, and thus the whole band can be divided into different channels, so that the system can use all these channels for transmission. A channel is then defined by a spectral mask, which gives limits in terms of power spectral density of the emitted signal. Fitting to those masks is the first step to ensure low interference in the system, and to evaluate the spectrum pollution due to our system.

We summarize the characteristics of the different considered frequency bands in Table 4-2. The authorized frequency bands and the maximum transmitted power in those bands are set by regulatory organisation, and can be found in documents emitted by FCC or ECC. The channel spacing and the corresponding spectral masks are on the contrary defined by the different standards, and can be found in the documents defining these standards.

Frequency Band (MHz)	Channels and bandwidth (B)	Maximum transmitted power	Spectral mask
868-868.6 (ECC rules)	1 channel fc = 868.3MHz B = 0.6MHz	25 mW	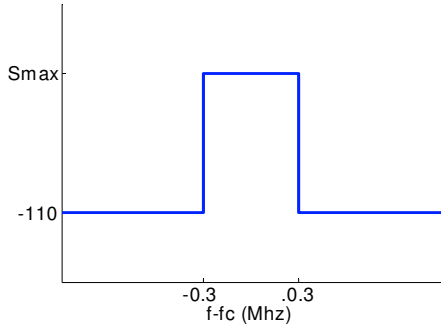
902-928 (FCC rules)	10 channels fc = 906 +2k MHz B = 2MHz	1000 mW	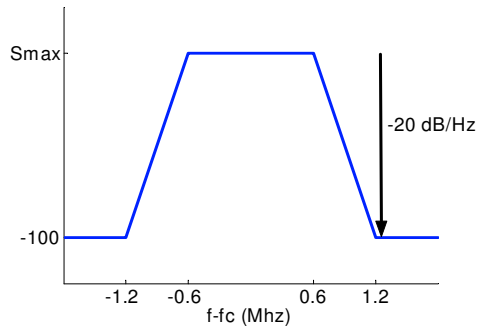

Zigbee 2400-2483.5	16 channels fc = 2405 +5k MHz B = 5MHz	100 mW	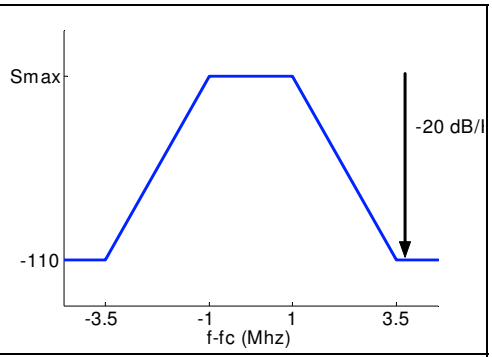
Bluetooth 2400-2483.5	79 channels fc = 2402 +k MHz B = 1MHz	100 mW	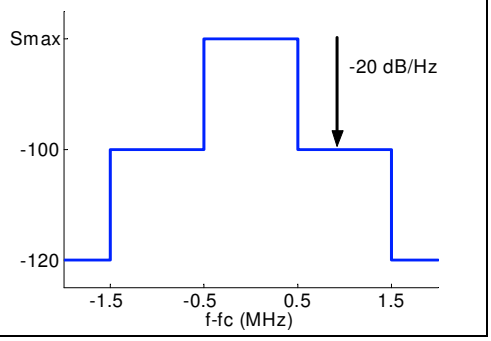

Table 4-2: Regulation and standards.

We should notice here that standards also define the modulation scheme, the transmitted power, the bit rate to use, and all other needed parameters. However in the objective of the Human++ program, we want to make comparison between different systems. So we keep the definition of the spectral masks, given by the different standards, and used them for other kind of modulations.

In the future, IMEC may develop its own standard for its body area network, and define which channel spacing and which spectral masks have to be used for IMEC standard. However it hasn't been done yet. The aim of this study is to show how we can compare different system configurations when we know the spectral mask. Therefore the spectral masks of others standards are taken here as examples, and may be changed in the future.

4.2.2 Fit to the mask

Once we know the spectral mask the emitted signal should fit in, we use the Matlab simulation tool developed in Section 3.5 to get an estimate of the signal spectrum and find the highest bit rate we can reach.

The performance of the system is fixed, and so the E_b/N_0 at the receiver is fixed. As mentioned above, increasing the bit rate will therefore increase the power and the spectrum occupancy of the signal. With an iterative method we can find the highest bit rate, which gives a signal whose spectrum, is under the mask and whose power doesn't exceed the maximum authorized transmitted power.

An example showing the evolution of the spectrum with the increasing of the bit rate is given in Figure 4.2. This example was done with a MSK modulation, a path loss of 90 dB, and a BER of 10^{-3} at the receiver. We can see that when the bit rate increases, the bandwidth of the emitted signal increases as well. For high bit rates (1 Mb/s) the signal power spectrum is outside of the spectral mask, and we don't fill the requirements anymore.

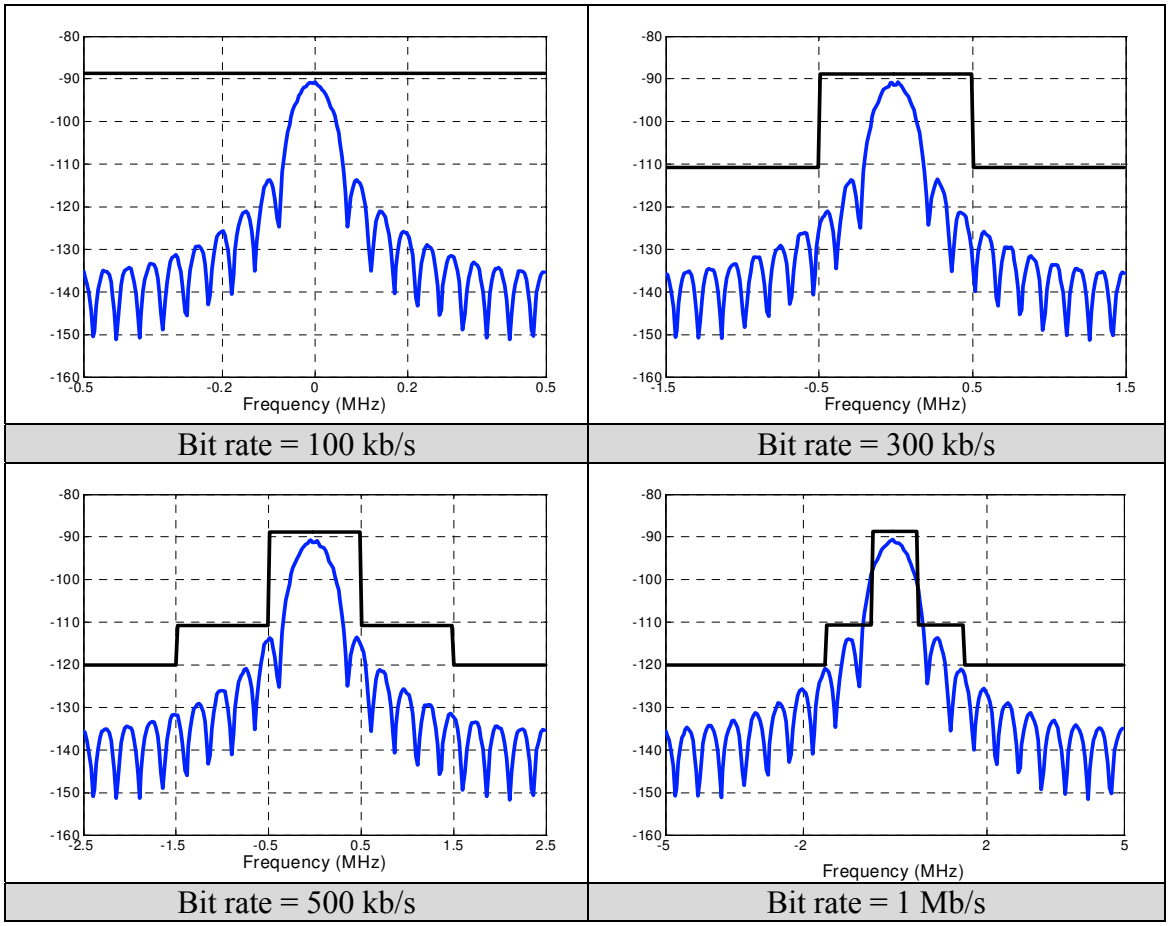

Figure 4.2: Evolution of spectrum while increasing the bit rate.

We have now two parameters on which the power consumption depends: the minimum required energy per bits, given by Equation (4.6), and the maximum achievable bit rate, computed with Matlab. For a given modulation we will therefore find the set of parameters that minimize the ratio $E_{b\text{-}tot}/R_b$, and then make comparison between the different optimized modulations.

Since the amount of possible choice for modulations, type of filters, or spectral masks is very large, we limited our study to some relevant examples.

4.3 Tested modulations

To make comparison in the different frequency bands, we chose to keep the distinction between linear and non-linear modulations in the two standards. So we used the spectral masks of the Zigbee standard with linear modulations and the spectral masks for the Bluetooth standard with continuous phase modulations. This limitation must be seen more as an example of comparison between different systems rather than as an extensive study on the choice of modulation for body area network.

As a matter of fact, the studies performed in the Human++ program in IMEC are still in the preliminary phase. Other comparative studies, more complete and more realistic, will follow in the future, and conclude about the choice of modulation. However the method described here can be seen as the basis for future work, and will be clearer with our examples.

Table 4-3 presents all the parameters we used for the simulations. At the receiver, we want to reach a bit error rate of 10^{-3}. We chose an antenna position of 90

degrees for all systems, and the path loss of the channel was computed with this value and the measurements of Section 3.3.1. The variable is the parameter we try to tune in order to minimize the value of $E_{b\text{-}tot}/N_0$.

Frequency band	Modulations	Default parameters	Variable
Zigbee 902	BPAM	Square root raised cosine with roll off = 0.3	Input back off
	16QAM		
Zigbee 2400	BPAM		
	16QAM		
Bluetooth 2400	Binary CPFSK	PA efficiency of 80%	Modulation index
	Binary GFSK	Bandwidth product BT = 0.5 PA efficiency of 80%	

Table 4-3: Modulations used for the simulations.

The default filters were chosen according to what is usually done in practice. For non-linear modulations, we always used Viterbi detector for the reception. This detector may require more power than other detectors presented in Section 2.4.3. However we suppose here that the receiver is not limited in terms of power consumption, and we are only interested in decreasing the power consumed at the transmitter. So we chose the detector offering the best performance.

The next section will now present the results we get with those modulations.

5 Simulation results

For each frequency and each modulation, we used the Matlab simulator developed in Section 3 to find the two decision parameters: the total energy consumed at the transmitter during the transmission of one bit and the maximum achievable bit rate. The modulation is considered as optimal when the ratio $E_{b\text{-}tot}/R_b$ is minimal (see Section 4). The results are presented in different graphs, showing the evolution of $E_{b\text{-}tot}/R_b$ (in dB) as a function of a system variable (see Table 4-3).
We will first compute the optimal parameters for each modulation in each band, and then make a global comparison of all optimized systems. The different graphs we produce may not give absolute values of the actual power consumption at the transmitter, but they reflect the behaviour of the different modulations in the body area network system.

5.1 Zigbee 902 band

We use in this band two different linear modulations (BPAM and 16-QAM), and the spectral mask given in Table 4-2. We want here to choose the best value for the input backoff of the power amplifier. This value influences both the signal distortion and the PA efficiency, and the trade-off between those two parameters is not the same for all modulations. The simulation in Matlab gives the graph of Figure 5.1.

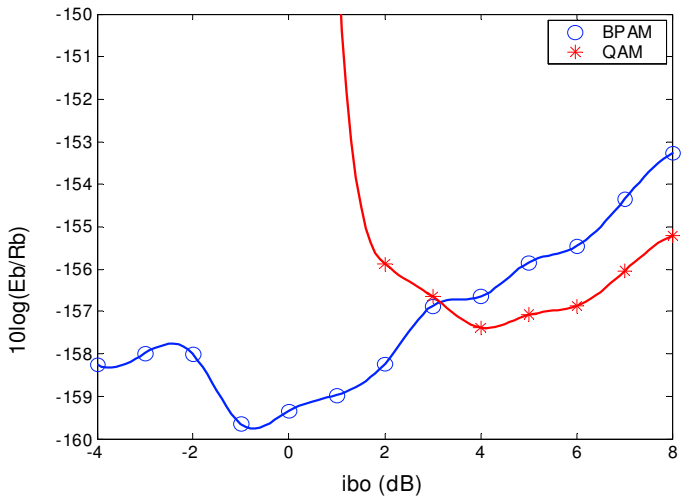

Figure 5.1: Modulation optimisation in the Zigbee 902 band.

The input back off of the PA influences the performances in different ways. High input back off leads to high linearity of the PA. This high linearity gives good performance at the receiver, so the required E_b/N_0 at the receiver is small. The high linearity guarantees also that the side lobes in the signal spectrum are small (see Section 3.2.2), and so we can reach high bit rates. On the other hand a high value of the input backoff gives low value for the PA efficiency, and the PA consumes more energy.

As far as 16-QAM is concerned, small input backoff, resulting in high non-linearity of the PA, will lead to significant compression in the signal constellation and distortion of the signal constellation (see Figure 3.7). Very important E_b/N_0 will be necessary to reach a BER of 10^{-3}. This appears on the curve, were $E_{b\text{-}tot}/R_b$ becomes very large for $IBO < 0$. The curve reaches then a minimum for $IBO = 4dB$. Increasing the input backoff further won't improve the BER performance or the maximum bit rate enough to compensate for the PA efficiency degradation. The best trade-off between linearity and efficiency of the PA is obtained for the input backoff of 3dB.

As far as BPAM is concerned, the signal constellation is less sensitive to compression than in the case of 16-QAM. We can work with lower input backoffs. The minimum value for $E_{b\text{-}tot}/R_b$ is obtained with $IBO = -1dB$. With higher input backoff, the PA efficiency decreases, and the energy per bit $E_{b\text{-}tot}$ increases. With smaller input backoffs, the side lobes of the emitted signal become more important, we need to lower the bit rate to make the signal fit to the mask.

This example shows clearly that the input backoff of the amplifier should be adjusted regard for the modulation. Modulations with few symbols are less sensitive to distortion and can work with lower input backoff than modulations using a large amount of symbols. The optimal input backoff should give acceptable signal distortion while being small enough to improve PA efficiency.

5.2 Zigbee 2400 band

We used the same modulations as in the previous example. But the spectral mask has been changed, according to Table 4-2. We also studied here the influence of the input backoff of the amplifier on the criterion $E_{b\text{-}tot}/R_b$. The graph on Figure 5.2 was produced with Matlab.

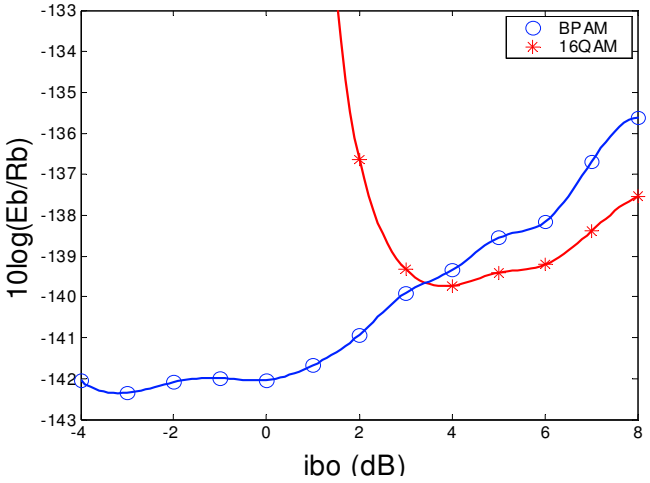

Figure 5.2: Modulation optimisation in the Zigbee 2400 band.

We didn't change the modulations, so the input backoff influence on BER performances and PA efficiency is the same as in the previous example. The difference here comes from the spectral mask and thus from the maximum bit rate.

The spectral mask used in the 2400 MHz band is much larger than the one from the 902 MHz band (see Table 4-2). So even with large side lobes in the emitted signal, we can reach high bit rates while fitting to the mask.

For 16-QAM, the change in spectral mask doesn't change the shape of the curve. This is because for low input backoffs, where the influence of side lobes is the most important, the degradation in BER performance dominates. The optimum input backoff is still obtained at $IBO = 4dB$. Beyond, the loss in PA efficiency dominates, and $E_{b\text{-}tot}/R_b$ is rising.

For BPAM on the contrary, the optimum IBO is decreased compare to the previous case, and is obtained for $IBO = -3dB$. In the 902Mhz band, the side lobes avoided the use of high bit rates for low input backoffs. With a wider spectral mask, as in the 2400 MHz band, large side lobes are not as restrictive. Even with important distortion, we can reach high bit rates and fit to the mask. Then the use of low input back offs is interesting since it gives better efficiency for the PA.

Depending on the spectral mask we chose, the optimum parameters for the PA can be modify. Larger spectral mask allowed more distortion in the signal spectrum and so allowed the use of lower input backoffs, which improves the PA efficiency.

5.3 Bluetooth 2400 band

In the same spectral band as before, we compare two different non-linear modulations: CPFSK and GFSK. In the Matlab simulation we computed the value of the decision criterion $E_{b\text{-}tot}/R_b$ for different values of the modulation index h (see Section 2.2.2 for a description of modulations). The results are shown on the graph below.

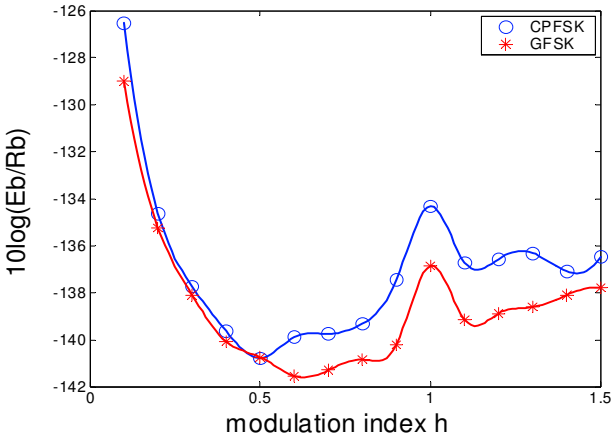

Figure 5.3: Modulation optimization in Bluetooth 2400.

Several comments can be made about these curves. First the curve for GFSK is always below the curve for CPFSK. The BER performances for both modulations are the same when using a Viterbi detector. On the opposite, we noticed in Section 2.2.2 that the use of gaussian filter reduces the spectral occupancy of the emitted signal. Therefore GFSK modulation can reach higher bit rates than CPFSK modulation, and so the ratio $E_{b\text{-}tot}/R_b$ is smaller for gaussian modulation.

Secondly a peak appears for the modulation index $h = 1$. This agrees with the example we presented in Section 2.4.3. We noticed there that the minimum distance

in the trellis, which determines the BER performance of the modulation, was quite low for $h = 1$, and that this modulation index results in poor performances So for $h = 1$, the minimum E_b/N_0 required at the receiver is quite important, and leads to a large value of $E_{b\text{-}tot}/R_b$.

Finally, and taking back the example of Section 2.4.3, we see that the optimal modulation index for our criterion is different from the optimal modulation index for a minimum distance criterion. Actually the modulation index giving the best performances in terms of BER was $h = 0.7$. But here we took into account the spectral performance of the signal. Low modulation index gives more compact spectrum, and so higher possible bit rates. This explains why the optimal modulation index we find here are below the value of 0.7.

The trade-off between a compact spectrum and good BER performance is given by the minimum of the curves. For CPFSK modulation, we reach the minimum for $h = 0.5$, leading to MSK modulation in that case. For GFSK modulation, the minimum is obtained for $h = 0.6$.

This example shows how the criterion we chose can modify the classical optimal parameters of different modulation. The choice of the index h for non-linear modulations has to take into account both BER performances and the shape of the signal spectrum.

As a final step in the systems comparison, we can now compare all the modulations with optimised parameters, in the different frequency bands.

5.4 Comparison of the 3 bands

We will now derive the total energy consumption per bit at the transmitter. This energy depends on two parameters: the energy consumed in the processing to generate the modulated signal with the desired energy, and the energy consumed by the front end during the transmission. With the Matlab simulation, we computed the signal energy required at the output of the transmitted antenna $E_{b\text{-}Tx}$, the efficiency of the PA used in the transmitter η, and the maximum achievable bit rate R_b. The total energy consumption is then given by

$$\xi = \frac{E_{b-Tx}}{\eta} + \frac{P_{FE}}{R_b} \tag{5.1}$$

where P_{FE} is the global power consumption of the front-end components.

P_{FE} should depend on the architecture of the front end used for the modulation. Other groups in IMEC are working on getting those data, but we don't have them yet. However, to get an idea of what a global system comparison looks like, we chose arbitrarily a value of $P_{FE} = 1mW$ for all modulations.

With this model we computed the value of the energy defined by Equation (5.1) for the different modulations of Table 4-3. The result shows the different proportion of energy consumption along the communication chain, and is presented on the figure below.

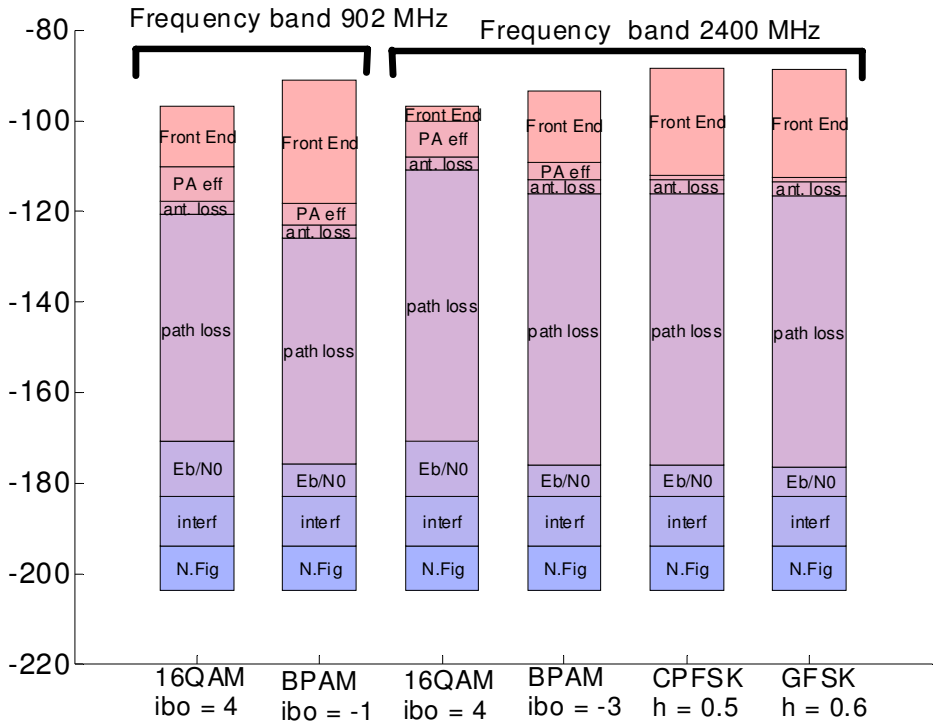

Figure 5.4: Total energy consumption for different modulations.

Some general comments about the modulations comparison can be made. First it appears that most of the energy is lost in the channel, so the choice of the carrier frequency and of the antenna positions will be very important in designing a body area network system.

Secondly we see in both frequency bands that 16-QAM needs more energy for the PA and for the ratio E_b/N_0 than BPAM. On the other hand, higher bit rates are achievable with 16-QAM, so the energy consumed by the front end is much lower than for BPAM. The decision of the best modulation will thus depend on the real value of the power consumption of the front end. In our case, with an equal P_{FE} for both modulations, 16-QAM seems more interesting than BPAM.

Thirdly, the choice of the standard and of the spectral mask also influences the energy consumption. Using a large spectral mask, as Zigbee 2400, allows the system to work at higher bit rates, than with a narrow spectral mask, as Bluetooth 2400. This results in more energy consumed by the front end when using Bluetooth mask than when using Zigbee mask. We can see this effect here when comparing linear and non-linear modulations in the 2400 MHz frequency band. On the other hand, having narrower spectral mask gives more available channels in the frequency band (see Table 4-2). We didn't take this parameter into account in this model, but it will certainly be investigated in the future.

We recall here that this example doesn't intend to conclude on the systems comparison. Other modulations need to be tested, further models need to be

developed, and we need to collect data on propagation around the human body and power consumption of front ends. However it shows what kind of results we can expect and how a complete comparison can be done. Even if the data are not really accurate yet, the method used to derive the global energy consumption can still be used.

6 Conclusions

6.1 Summary

The work developed in this thesis is a part of the more global project led in IMEC to design a wireless network around the human body. The key parameter ruling this design is very low power consumption of the sensors placed on the body. Done in the early phase of the project, this thesis contributed to the development of a simulation tool for the body area network. The work presented here has had mainly two applications in the frame of the Human++ program.

First we implemented a rather complete end-to-end model of the communication link. With a large amount of parameters to test, for modulations or for system non-idealities, the simulation tool will be used in the future to make other studies than the examples presented in this thesis.

Secondly we identified some of the parameters that will influence the power consumption of the system, such as BER performance, efficiency of the system or maximum achievable bit rates. The method used to estimate the total energy consumed by the transmitter during the emission of one bit shows what are the different parts of the communication chain responsible for power losses, and this method can still be used when new results will show up in the Human++ program.

6.2 Future work

As a part of a research program, the work of this master thesis doesn't intend to close the question of the optimal design for body area network. As we saw in Section 5, the results we can obtain at the present time remains very general, and we still need to improve some parts of our model to get more accurate simulations.

First an important work is done in IMEC to develop new models for channels, taking into account the specificity of propagation around the human body. With mathematical models fitting to measurements or with impulse responses of this channel, the simulation will be more realistic, and we can better study the performance of the network.

Secondly a model for the interferences in the channel seems necessary. Obviously all modulations won't produce the same amount of interferences in adjacent channel. Contrary to what as been done in this thesis, interference level will vary with the choice of the system, and so some systems will have their performances more decreased than other. A more complete system comparison should therefore include this varying interference level.

Thirdly, as mentioned in our example, we need to collect data about the different front-end power consumptions, to get realistic comparison between the energy consumed at the front end for different modulations. The constant value we used in this work was useful to present a global comparison of systems, but is of course not reflecting the real world.

Finally, we can think of some improvements of the end-to-end model, by adding other blocks used in real communication systems, such as synchronization or channel estimation. In a further step, the simulation will have to include the whole network, by considering transmission from all the sensors to the base station.

All these ideas for future work will of course be investigated in the frame of the Human++ program in IMEC. Inside this program, many other issues are and will be considered, such as the miniaturization of sensors, the increasing of lifetime of the batteries, the power devices used for the sensors, the processing of collected data… Exciting challenges await the people working on Human++ program.

7 Abbreviations

AWGN.....Additive White Gaussian Noise
BAN.....Body Area Network
BER .....Bit Error Rate
CPFSK .....Continuous Phase FSK
CPM .....Continuous Phase Modulation
ECC .....Electronic Communications Committee
FCC .....Federal Communication Commission
FE .....Front End
FSK.....Frequency Shift Keying
GFSK.....Gaussian FSK
IBO .....Input BackOff
ISI .....InterSymbol Interference
MSK .....Minimum Shift Keying
PA .....Power Amplifier
PAM .....Pulse Amplitude Modulation
PLL.....Phase Locked Loop
PSD.....Power Spectral Density
QAM.....Quadrature Amplitude Modulation
SNR.....Signal to Noise Ratio
VCO.....Voltage Controlled Oscillator

8 Bibliography

[1] T. S. Rappaport, *Wireless Communications*, Prentice Hall PTR, Upper Saddle River, NJ, 1996.

[2] John G. Proakis, *Digital Communications Third Edition*, McGraw-Hill, New York, 1995.

[3] J. B. Andersson, T. Aulin, and C. E. Sundberg, *Digital Phase Modulation*, Plenum Press, New York, 1986.

[4] T. Aulin and C. E. Sundberg, *Continuous Phase Modulation: Part I-Full response signaling*, IEEE Trans. on Commun., vol. COM-29, pp. 196-209, Mar. 1981.

[5] T. Aulin, N. Rydbeck, and C. E. Sundberg, *Continuous Phase Modulation: Part II-Partial response signaling*, IEEE Trans. on Commun., vol. COM-29, pp. 210-225, Mar. 1981.

[6] C. E. Sundberg, *Continuous Phase Modulation*, IEEE Communications Mag., vol. 24, no.4, pp. 25-38, April 1986.

[7] G. D. Forney, *The Viterbi algorithm*, Proc. IEEE, vol. 61, pp 268-278, Mar. 1973.

[8] A. Svensson, C. E. Sundberg, and T. Aulin, *A class of reduced-complexity Viterbi detectors for partial response continuous phase modulation*, IEEE Trans. on Comm., vol. 32, no. 10, pp. 1079-1087, Oct. 1984.

[9] A. Svensson, *Reduced state sequence detection of partial response continuous phase modulation*, IEEE Proc., vol. 138, no. 4, pp. 256-268, Aug. 1991.

[10] T. Svensson, A. Svensson, *Reduced complexity detection of bandwidth efficient partial response CPM*, IEEE 49th Vehicular Technology Conference, vol. 2, 16-20 May 1999.

[11] T. Larsson, *Optimal design of CPM decoders based on state-space partitioning*, IEEE Proc., International Conference on Communications, vol. 1, pp. 123-127, May 1993.

[12] L. Zihuai; T. Aulin, *Symbol error probability bounds for CPM signaling over AWGN channels*, IEEE International Conference on Communications, vol. 5, pp. 3467-3471, May 2003.

[13] T. Aulin, *Symbol error probability bounds for coherently Viterbi detected continuous phase modulated signals*, IEEE Trans. on Comm., vol. 29, Issue 11, pp. 1707-1715, Nov 1981.

[14] T. Svensson, A. Svensson, *Maximizing minimum Euclidean distance of spectrally constrained partial response CPM*, IEEE Vehicular Technology Conference, vol. 2, pp. 1244-1248, 6-9 May 2001.

[15] K. Murota, K. Hirade, *GMSK modulation for digital mobile radio telephony*, IEEE Trans. on Comm., vol. 29, Issue 7, pp. 1044 – 1050, Jul. 1981.

[16] T. Svensson, A. Svensson, *Empirical model for spectrally efficient continuous phase modulation*, IEEE Vehicular Technology Conference, vol.1, pp. 696-700, 6-9 Oct. 2003.

[17] S. Pasupathy, *Minimum shift keying: a spectrally efficient modulation*, IEEE Communications Mag., vol. 17, no. 4, pp. 14-22, July 1979.

[18] G. S. Deshpande and P. H. Wittke, *Optimum pulse shaping in digital angle modulation*, IEEE Trans. on Comm., vol. COM-29, vol. 2, pp. 162-168, Feb. 1981.

[19] S. M. Elnoubi, *Probability of error analysis of digital partial response continuous phase modulation with noncoherent detection in mobile radio channels*, IEEE Trans. on Vehicular Technology, vol. 38, Issue 1, Feb. 1989.
[20] M. Simon, C. Wang, *Differential versus Limiter-Discriminator detection of narrowband FM*, IEEE Trans. on Comm., vol. COM-31, nov. 1983.
[21] O. Andrisano, M. Chiani, R. Verdone, *Performance of narrowband CPM systems with limiter-discriminator-integrator detection and decision feedback equalization in mobile radio channels*, IEEE Trans. on Vehicular Technology, vol. 42, Issue 2, May 1993.
[22] A. Viterbi, *Error bounds for convolutional codes and an asymptotically optimum decoding algorithm*, IEEE Trans on Information Theory, vol. 13, Issue 2, pp. 260-269, April 1967.
[23] A. Trachtman, I. Kalet, S. Shamai, *Limiter-discriminator detection of continuous phase modulation*, IEEE Trans on Comm., vol. 42, issue 234, pp. 819 825, April 1994.
[24] T. Svensson. *On spectrally efficient continuous phase modulation*, Licentiate Thesis 363L, Department of Signals and Systems, Chalmers University of Technology, Göteborg, Sweden, Nov. 2000.
[25] P. Robertson and S. Kaiser, *Analysis of the effects of phase noise in orthogonal frequency division multiplex (OFDM) systems*, IEEE International Conference on Communications, vol. 3, pp. 1652–1657, June 1995.
[26] A. G. Armada and M. Calvo, *Phase noise and sub-carrier spacing effects on the performance of an OFDM communication system*, IEEE Communications Letters, January 1998.
[27] R. Hasholzner, C. Drewes, and J. S. Hammerschmidt, *The effects of phase noise on 26 Mb/s OFDMA broadband radio in the local loop systems*, Proceedings ACTS Mobile Communications Summit, pp. 105–112, October 1997.
[28] C. Muschallik, *Influence of RF oscillators on an OFDM signal*, IEEE Trans. on Consumer Electronics, COM-41, pp. 592–603, August 1995.
[29] B. Come, R. Ness, S. Donnay, L. Van der Perre, W. Eberle, P. Wambacq, M. Engels, and I. Bolsens, *Impact of front-end non-idealities on bit error rate performance of WLAN-OFDM transceivers*, Microwave Journal, pp. 126–140, February 2001.
[30] N. J. Kasdin, *Discrete simulation of colored noise and stochastic processes and $1/f^{\alpha}$ power law noise generation*, IEEE Proc., vol. 83, pp. 802-827, May 1995.
[31] P. Balaban, M. C. Jeruchim and K. S. Shanmugan, *Simulation of communication systems*, Plenum Press, 1992.
[32] V. Kroupa, *Noise properties of PLL systems*, IEEE Trans. on Comm., vol. 30, pp. 2244–2252, October 1982.
[33] B. Razavi, *RF Microelectronics*, Prentice Hall, 1998.
[34] A. Saleh, *Frequency-independent and frequency-dependent nonlinear models of TWT amplifiers*; IEEE Trans. on Comm., vol. 29, Issue 11, pp. 1715-1720, Nov 1981.
[35] S. Pupolin, L. Greenstein, *Performance analysis of digital radio links with nonlinear transmit amplifiers*, IEEE Journal on Selected Areas in Communications, vol. 5, Issue 3, pp. 534-546, April 1987.
[36] Cheng-Po Liang, Je-Hong Jong, W. E. Stark, J. R. East, *Nonlinear amplifier effects in communications systems*, IEEE Trans. on Microwave Theory and Techniques, vol. 47, Issue 8, pp. 1461-1466, Aug. 1999.
[37] J. Minkoff, *The role of AM-to-PM conversion in memoryless nonlinear systems*, IEEE Trans. on Comm., vol. 33, Issue 2, pp. 139-144, Feb 1985.

[38] J. Boccuzzi, *Performance evaluation of non-linear transmit power amplifiers for North American digital cellular portables*, IEEE Trans. on Vehicular Technology, vol. 44, Issue 2, pp. 220-228, May 1995.
[39] M. Sanchez, L. de Haro, A. Pino, and M. Calvo, *Human operator effect on wide-band radio channel characteristics*, IEEE Trans. on Antennas and Propagation, vol. 45, Issue 8, pp. 1318-1320, August 1997.
[40] T. B. Welch, R. L. Musselman, B. A. Emessiene, P. D. Gift, D. K. Choudhury, D. N. Cassadine, and S. M. Yano, *The effects of the human body on UWB signal propagation in an indoor environment*, IEEE Journal on Selected Areas in Communications, vol. 20, No. 9, pp. 1778-1782, December 2002.
[41] T. Zasowski, F. Althaus, M. Stager, A. Wittneben, G. Troster, *UWB for non-invasive wireless body area networks channel measurements and results*, IEEE Conference on Ultra Wideband Systems and Technologies, pp. 285-289, 16-19 Nov. 2003.
[42] ERC Recommendation 70-03, *Relating to the use of Short Range Devices*, April 2002, http://www.ero.dk.
[43] FCC Code of Federal Register (CFR), Part 47, Section 15.205, Section 15.209, Section 15.247, and Section 15.249, http://www.fcc.gov/oet/info/rules.
[44] ETSI EN 300 220-1, *Electromagnetic Compatibility and Radio Spectrum Matters (ERM); Short Range Devices (SRDs);Part 1.*
[45] IEEE Std 802.15.4-2003, Part 15.4, *Wireless Medium Access Control (MAC) and Physical Layer (PHY) Specifications for Low-Rate Wireless Personal Area Networks*, IEEE Standard for Information technology, April 2003.
[46] ERC Report 109, *Compatibility of Bluetooth with other existing and proposed radio communication systems in the 2.45 GHz frequency band.*
[47] E. H. Newman, P. Bohley, and C. H.Walter, *Two methods for the measurement of antenna efficiency*, IEEE Trans. on Antennas Propagation, vol. 23, pp. 457–461, July 1975.